Contrib Mineral Petrol (2012) 163:897–921
DOI 10.1007/s00410-011-0705-5

ORIGINAL PAPER

Timing of high-pressure metamorphic events in the Bulgarian Rhodopes from Lu–Hf garnet geochronology

M. Kirchenbaur · J. Pleuger · S. Jahn-Awe · T. J. Nagel · N. Froitzheim · R. O. C. Fonseca · C. Münker

Received: 11 May 2011 / Accepted: 22 October 2011 / Published online: 2 December 2011

Abstract Within the Mediterranean realm, the Rhodopes represent a nappe stack of oceanic and continental fragments assembled along the Eurasian continental margin during the Alpine orogeny. The timing of the high-pressure (HP) metamorphism has long been ambiguous, lacking detailed geochronological and geochemical control on subduction-exhumation and nappe stacking processes. Here we apply the Lu–Hf and Sm–Nd chronometers to a suite of representative eclogite samples covering two different key units of the Rhodopean nappe stack: (1) the Kimi Complex (Upper Allochthon) and (2) the Middle Allochthon. In addition to geochronology, we also determined whole rock Hf and Nd isotope compositions as well as major and trace element concentrations in order to constrain the nature of the eclogite protoliths. Two HP metamorphic events were revealed by Lu–Hf geochronology: (1) a Lower Cretaceous event in the Upper Allochthon (126.0 ± 1.7 Ma) and (2) an Eocene event in the Middle Allochthon (44.6 ± 0.7 Ma; 43.5 ± 0.4 Ma; 42.8 ± 0.5 Ma), at conditions of ca. 700°C/20–25 kbar. Our new data provide direct evidence for multiple subduction events in the Rhodopes. Exhumation and subsequent thrusting of the Middle Allochthon on the Lower Allochthon can be narrowed down to the time span between 42 and 34 Ma. In a broader tectonic context, the Eocene ages for the HP metamorphism support the view that the Rhodopes represent a large-scale tectonic window, exposing the deepest nappe units of the Hellenides.

Keywords Geochronology · Eclogite · Lu–Hf · Sm–Nd · HP metamorphism · Rhodopes

Communicated by J. Hoefs.

Electronic supplementary material The online version of this article (doi:10.1007/s00410-011-0705-5) contains supplementary material, which is available to authorized users.

M. Kirchenbaur (✉) · S. Jahn-Awe · T. J. Nagel · N. Froitzheim · R. O. C. Fonseca
Abteilung für Endogene Prozesse, Steinmann-Institut, Universität Bonn, Poppelsdorfer Schloss, 53115 Bonn, Germany
e-mail: Kirchenbaur@uni-bonn.de

M. Kirchenbaur · C. Münker
Institut für Geologie und Mineralogie, Universität zu Köln, Zülpicher Strasse 49b, 50674 Köln, Germany

J. Pleuger
ETH Zürich, Geologisches Institut, Sonneggstrasse 5, 8092 Zürich, Switzerland

Introduction

The convergence between Africa and the Eurasian continent since the Jurassic led to the closure of the Tethyan realm in a protracted succession of subduction and collision events involving several microplates (Stampfli and Borel 2002; van Hinsbergen et al. 2005). In this context, rock units of both oceanic and continental affinity were subducted and metamorphosed at high-pressure (HP) and even ultra-high pressure (UHP) conditions (e.g., Gebauer et al. 1997; Mposkos and Kostopoulos 2001), and subsequently they were exhumed and incorporated into the evolving Alpine orogen. Constraining the exact timing of these events as well as characterization of the protoliths involved is crucial for reconstructing the geodynamic evolution of the Eastern Mediterranean realm. The Rhodopes, which are exposed in southern Bulgaria and northern Greece (Figs. 1, 2), are a key locality to understand the succession of HP events in the eastern Mediterranean as they represent the link between the Hellenic-Dinaric thrust belt and the Eurasian continental margin.

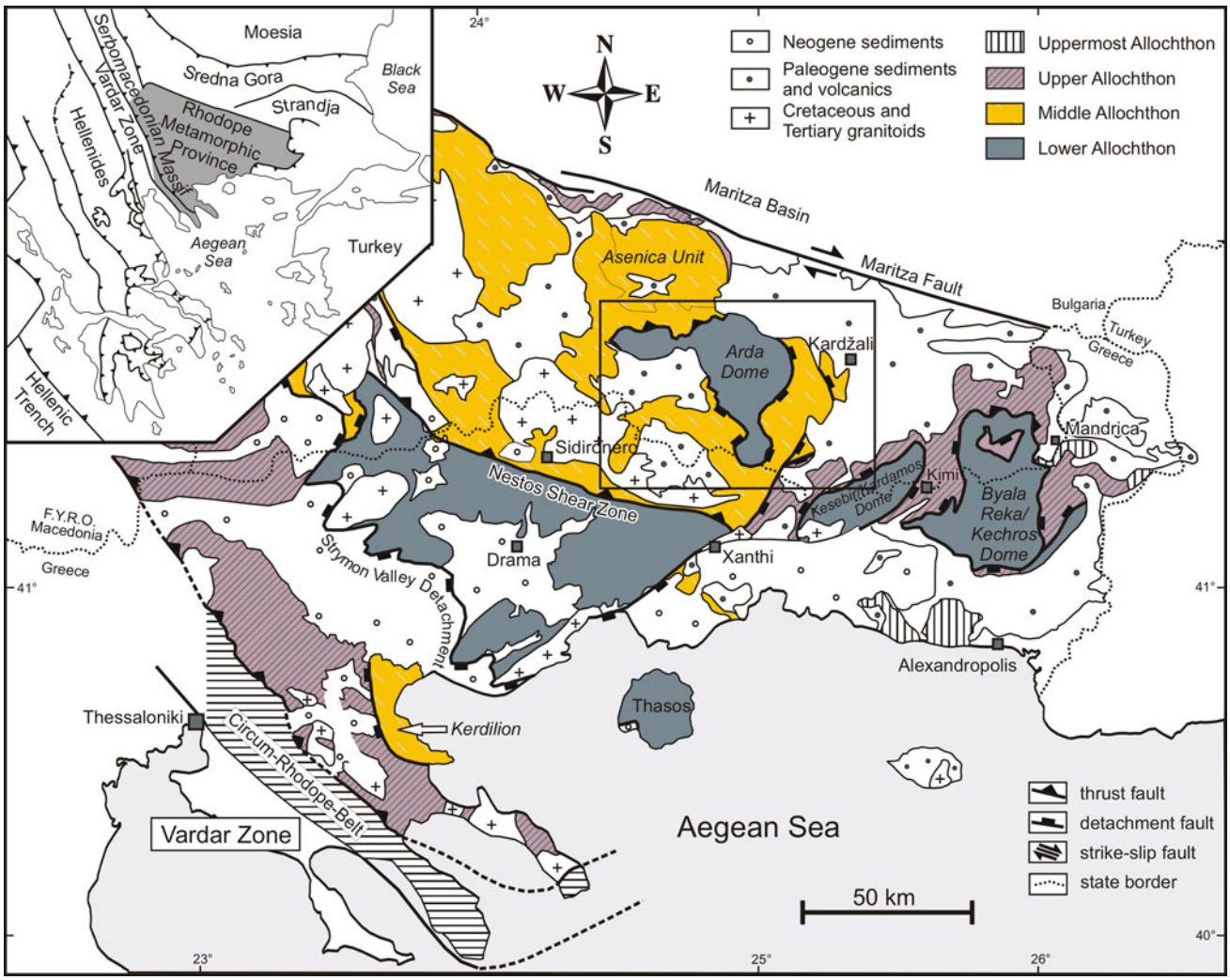

Fig. 1 Geological overview of the Bulgarian and Greek Rhodopes; modified after Tueckmantel et al. (2008) and Jahn-Awe et al. (2010). Marked field illustrates map shown in Fig. 2

In the Rhodopes, evidence for the presence of deeply subducted oceanic and continental fragments reaching up to UHP conditions has been discovered in eclogites, metapelites and mélange-zone rocks (Mposkos and Kostopoulos 2001; Perraki et al. 2006; Cornelius 2008; Schmidt et al. 2010; Janák et al. 2011). However, only limited geochronological and geochemical data for the eclogite-facies rocks are available so far, and the results are inconsistent. Based on zircon dating, Liati (2005) postulated four episodes of HP to UHP metamorphism whereas Krenn et al. (2010) argue that UHP metamorphism was confined to ca. 180 Ma, followed by decompression.

In the last two decades, direct dating of HP metamorphic events in Alpine or older metamorphic rocks has been improved by the application of the Lu–Hf (and Sm–Nd) geochronometers to metamorphic garnet (e.g., Vance and O'Nions 1990; Duchêne et al. 1997; Amato et al. 1999; Scherer et al. 1997, 2000; Blichert-Toft and Frei 2001; Thöni 2002; Lapen et al. 2003; Lagos et al. 2007; Herwartz et al. 2008, 2011; Smit et al. 2010). The major advantages of this approach are (1) high Lu/Hf (and Sm/Nd) ratios in garnet, (2) the additional information from initial Hf–Nd isotope compositions about the nature of the protolith and (3) the fact that garnet ages can be tied to specific P–T conditions. New analytical approaches (e.g., Lagos et al. 2007) also allow the selective digestion of garnet, thus minimizing the effects of inclusions that are in isotopic disequilibrium with the host garnet.

In this study, we present Lu–Hf and Sm–Nd isotope data for whole rocks and omphacite/garnet mineral separates for four eclogite samples from two different tectonic units of

the Bulgarian Rhodopes. These data are complemented by element profiles of garnet obtained by LA-ICP-MS and electron microprobe, whole rock major and trace element analyses and are furthermore combined with petrological observations and phase diagram calculations. The results lead to a fundamental tectonic re-interpretation of the Rhodopes as the most internal portion of the Hellenides rather than an independent older orogen.

Geological overview

The Rhodopes are tectonically sandwiched between the Hellenic-Dinaric thrust belt in the south-west and the Eurasian continental margin, including the Balkanides, to the north (Fig. 1). To the south, the Rhodopes extend into Greece and are partially covered by the Aegean Sea. The present study focuses on the Bulgarian part of the Rhodopes, which is built of several metamorphic thrust units that were re-structured by intense extension in the Eocene and Miocene (e.g., Burg et al. 1996; Kilias et al. 1999; Krohe and Mposkos 2002; Bonev et al. 2006; Pleuger et al. 2011). The extensive nomenclature for individual, local units so far lacks a consistent classification scheme. Here, we follow the approach of Janák et al. (2011), referring to four large superunits: the Lower, Middle, Upper and Uppermost Allochthon (Figs. 1, 2). The nomenclature introduced by Janák et al. (2011) also allows a direct tectonic correlation between the Rhodopes in the strict sense and the Serbo-Macedonian Massif further south-west. A short description of the respective units along with the most important available geochronological data is given in Table 1.

The *Lower Allochthon* is exposed south of the Nestos Shear Zone ("Rhodope Metamorphic Core Complex" or "Pangaion–Pirin Complex"; Dinter and Royden 1993; Dinter 1998; Georgiev et al. 2010; Jahn-Awe et al. 2010) as well as in three metamorphic core complexes (Arda–Byala Reka/Kechros–Kesebir/Kardamos) that form extensive domes in the eastern part of the Rhodopes (Figs. 1, 2). The Lower Allochthon is composed of Variscan basement (e.g., Wawrzenitz and Mposkos 1997; Peytcheva et al. 2004; Ovtcharova et al. 2004; Turpaud and Reischmann 2010) and a metasedimentary sequence, reaching greenschist- to amphibolite-facies metamorphism in the Pangaion–Pirin complex and migmatization in the Arda, Byala Reka/Kechros and Kesebir/Kardamos complexes. Migmatization in the Arda dome took place at 37.8 ± 1.5 Ma (Cherneva et al. 2002).

The *Middle Allochthon* corresponds to the Sidironero-Mesta Unit in the broad sense and includes the Madan, Arda 2, Starcevo, Borovica and Asenica Units in the Central Rhodopes (Table 1; Figs. 1, 2). The Middle Allochthon is equivalent to the "Rhodope Terrane" of Turpaud and Reischmann (2010) and Jahn-Awe et al. (2010) and is a mixed unit of continental and oceanic affinity, including orthogneisses derived from Jurassic to Early Cretaceous arc granitoids, and intruded by Eocene granitoids (U–Pb on zircons; Ovtcharova et al. 2004; Turpaud and Reischmann 2010; Jahn-Awe et al. 2010). The metamorphic grade reached up to eclogite facies (e.g., Kolčeva et al. 1986; Liati and Mposkos 1990; Liati and Seidel 1996). Furthermore, mineral relics and mineral compositions indicating UHP metamorphic conditions have been reported from several different localities from the base of the Middle Allochthon (microdiamond inclusions in garnet of metapelites; Mposkos and Kostopoulos 2001; Perraki et al. 2006; Schmidt et al. 2010). The timing for thrusting of the Middle on the Lower Allochthon along the top-to-the-south-west Nestos Shear Zone was recently confined by Jahn-Awe et al. (2010) to 55–32 Ma. An Eocene activity of the Nestos Shear Zone is also constrained by ca. 42–38-Ma-old pegmatite veins affected by mylonitization along the Nestos Shear Zone (Liati 2005; Bosse et al. 2009).

The *Upper Allochthon* is composed of the Kardžali Unit and the Kimi Complex in the Eastern Rhodopes and the Vertiskos/Ograzhden Unit in the Serbo-Macedonian Massif, which is regarded as the western continuation of the Rhodopes (Table 1; Figs. 1, 2; Burg et al. 1996; Ricou et al. 1998; Himmerkus et al. 2009a, b). The Upper Allochthon is a composite unit made up of metapelites, gneisses, amphibolites, marbles and boudins of eclogites and ultramafic rocks. The latter have previously been interpreted as melting residues and cumulates emplaced at the base of a thickened crust (Baziotis et al. 2008). A metamorphic grade of eclogite facies up to UHP conditions has been documented for the Kimi Complex (Mposkos and Kostopoulos 2001). Recently, microdiamond inclusions in zircons were also reported from the mélange zone at the base of the Upper Allochthon by Cornelius (2008). So far, the timing of UHP metamorphism in the Upper Allochthon could only be constrained between 200 and 41 Ma and is still a matter of debate for the Kimi Complex. Most recently an Early Jurassic age (~180 Ma) was suggested by Krenn et al. (2010).

The *Uppermost Allochthon* consists of the Circum-Rhodope Belt as well as the Mandrica and Alexandropolis greenschists. These units consist of low-grade metamorphic sedimentary and volcanic rocks, partly of oceanic affinity and were thrust northwards over the Eurasian margin in the Late Jurassic to Early Cretaceous (Bonev and Stampfli 2003).

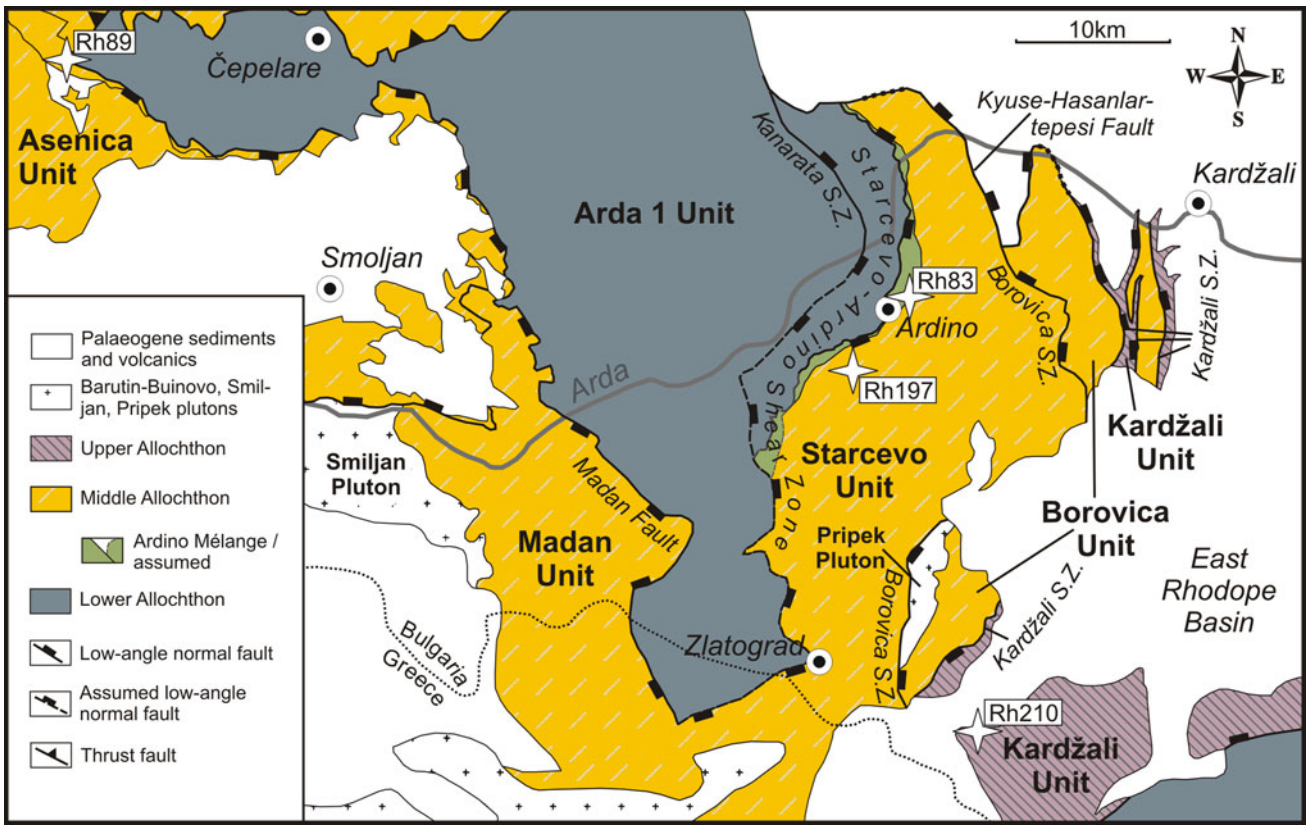

Fig. 2 Sample localities of the four studied eclogite samples: Rh-83, Rh-89 and Rh-197 from the *Middle Allochthon* (Starcevo Unit and Chepelare suture) and Rh-210 from the *Upper Allochthon* (Kardzali Unit). Modified after Jahn-Awe et al. (2011)

Sample localities

Three eclogite samples (Rh-83, Rh-89 and Rh-197) were taken from key localities in the Middle Allochthon and one sample (Rh-210) from the Upper Allochthon (GPS coordinates see Table 2). Rh-83 and Rh-197 were sampled near to each other, within the same sub-unit (Starcevo Unit of the Middle Allochthon; see Fig. 2).

Sample Rh-83 is of particular importance, in that it is a sapphirine-bearing kyanite eclogite. It has been collected in a small creek bed ~300 m north-east of the town of Ardino, located at the top of the Ardino Mélange (Fig. 2). This mélange forms the basal part of the Starcevo Unit (Middle Allochthon) and is characterized by ortho- and para-gneisses, marbles, amphibolites and minor ultramafic rocks and eclogites. On top of the mélange towards east follow mixed gneisses of the Starcevo Unit proper. As sample Rh-83 was part of a stream boulder, it is not clear whether its original tectonic position was in the uppermost part of the mélange or upstream in the hanging-wall of the mélange within the mixed gneisses of the Starcevo Unit that also contain eclogites.

Eclogite Rh-197 has been collected ~700 m to the north-east of Sransko village (south-west of Ardino; Fig. 2). It originates from lenses of amphibolite and eclogite enclosed in migmatitic gneisses of the Starcevo Unit.

Fig. 3 Results of the calculation of equilibrium phase diagrams for the samples Rh-83, Rh-89 and Rh-197. **a** Equilibrium assemblage diagram for the bulk composition of Rh-83 (Table 2) in an Si–Al-Ti–Fe–Mn–Mg-Ca–Na–K system with excess H_2O. *Grey-shaded* area corresponds to the observed high-pressure assemblage. (1) Grt + Phe + Cpx + Ctd + Lws + Rt + Qtz; (2) Grt + Phe + Cpx + Ctd + Rt + Qtz; (3) Grt + Phe + Cpx + Ctd + Am + Rt + Qtz; (4) Grt + Fsp + Phe + Am + Rt + Spn + Qtz; (5) Grt + Fsp + Phe + Am + Spn + Qtz; (6) Grt + Fsp + Phe + Cpx + Am + Rt + Qtz; (7) Grt + Fsp + Phe + Cpx + Rt + Qtz; (8) Grt + Fsp + Bt + Cpx + Am + Rt + Qtz; (9) Grt + Fsp + Bt + Am + Spn + Qtz. **b** Equilibrium assemblage diagram for the estimated composition of Al-rich coronae around decomposing kyanite in Rh-83 (Table 2) in an Si–Al-Ti–Fe–Mg–Ca-Na system. *Grey-shaded* area corresponds to the observed assemblage. (1) Grt + Fsp + Spl + Spr + Rt + Crn; (2) Fsp + Spl + Opx + Spr + Rt + Crn; (3) Fsp + Spl + Crd + Spr + Rt + Crn; (*A*) Boundary of stability field of Fsp + Spl + Spr + Rt + Crn with excess H_2O. **c** Equilibrium assemblage diagram for the bulk composition of Rh-89 (Table 2) in an Si–Al-Ti–Fe–Mn–Mg-Ca–Na–K system with excess H_2O. *Grey-shaded* area corresponds to the observed high-pressure assemblage. **d** Pressure–temperature path for the exhumation of the lower, eclogite-bearing part of the Middle Allochthon constrained by the high-pressure assemblage (see **a**) and Al-rich coronae (Pl + Spl + Rt + Spr + Crn; see **b**) observed in Rh-83, and Al-rich coronae (Pl + Ky + Spl + Spn + Crn) observed in Rh-197. **e** Equilibrium assemblage diagram for the bulk composition of Rh-210 (Table 2) in an Si–Al-Ti–Fe–Mn–Mg-Ca–Na–K system with excess H_2O. *Grey-shaded* area corresponds to the observed high-pressure assemblage. (1) Grt + Phe + Cpx + Am + Rt + Qtz; (2) Grt + Fsp + Cpx + Am + Rt + Spn; (3) Grt + Fsp + Cpx + Am + Rt

Eclogite sample Rh-89 originates from the so-called Čepelare Shear Zone (Fig. 2; Burg et al. 1990; Bosse et al. 2009; Gerdjikov et al. 2010), a mixed zone at the base of the Arda 2 Unit (Middle Allochthon). The sample has been collected ~1 km south-east of Beden village. At this locality, fine-grained eclogites and surrounding garnet-amphibolites form a 25-m-long and 10-m-thick boudin embedded in gneiss.

Eclogite sample Rh-210 originates from the Kardžali Unit, which is part of the Upper Allochthon (see Table 1). The sample has been collected ~3 km WNW of Drangovo village (Fig. 2). The sample originates from an eclogite boudin hosted by garnet-micaschists. More eclogite outcrops can be found towards north-north-east and south-south-west in a thin band on top of a west-north-west-dipping extensional shear zone.

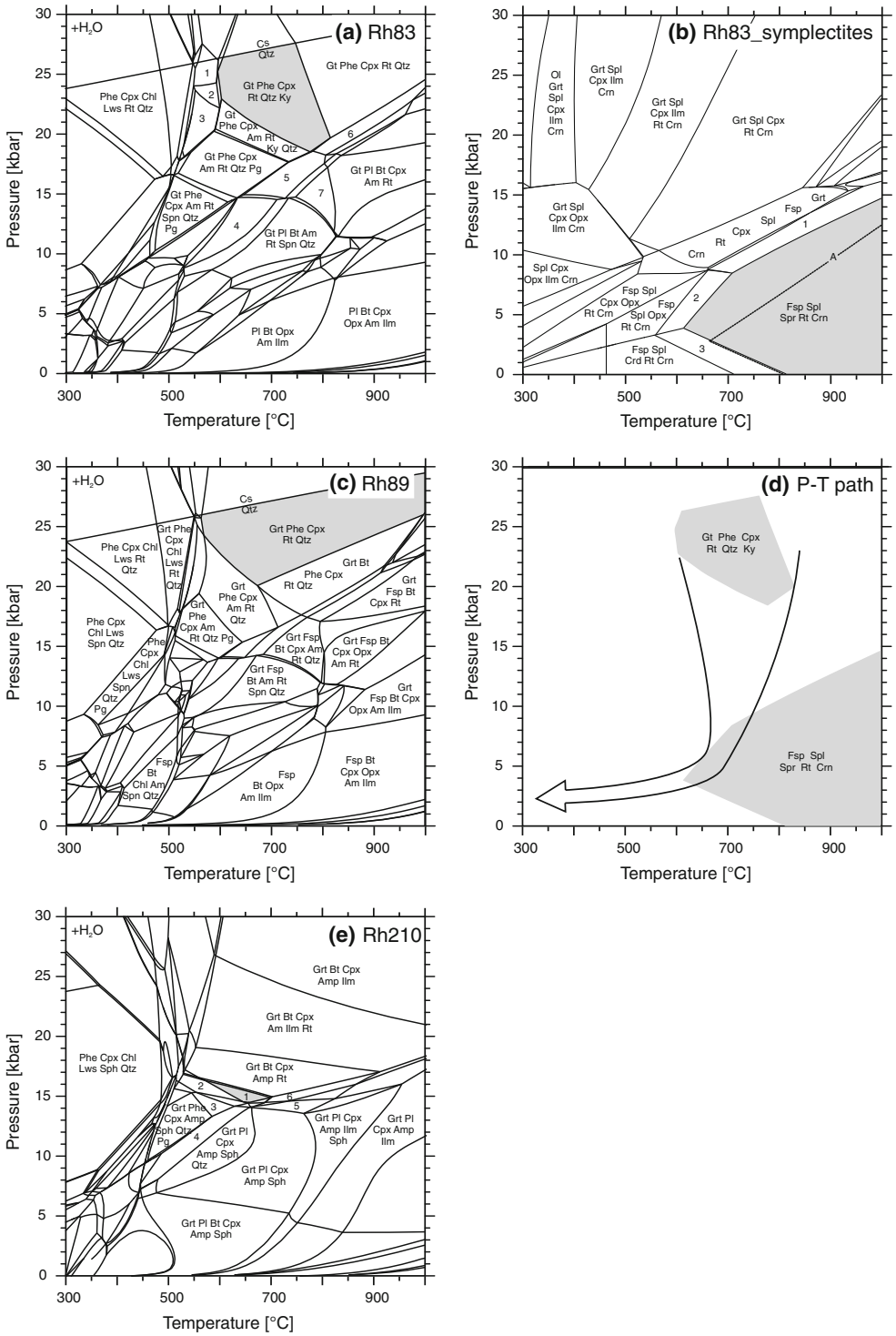

Analytical techniques

Sample preparation, separation and digestion

Four eclogite samples (Rh-83, Rh-89, Rh-197 and Rh-210) were analysed for their whole rock major and trace element concentrations as well as for Lu–Hf and Sm–Nd isotope compositions. The results along with GPS coordinates of sample localities are listed in Tables 2 and 3.

After removing the weathering crusts with a rock saw, the samples (total weight ca. 2–3 kg) were crushed in a steel mortar. A representative aliquot was then ground in an agate mill and the powder was subsequently used for bulk rock analyses. For trace element analyses, the sample powder was digested in a 1:1 mixture of HNO_3-HF in Parr bombs for 3 days to ensure complete sample digestion and was subsequently dried down with one mL of perchloric acid. A second aliquot of the crushed sample was sieved, and the fractions >63 μm were purified with a Frantz magnet separator. In order to prevent a selective separation of either garnet rim or core, the settings were adjusted to remove non-magnetic minerals only. Subsequently, three to five garnet separates per sample were hand-picked under a binocular lens. Both visibly inclusion-free and inclusion-bearing garnet fractions were separated in order to avoid biasing the results towards either garnet rims or cores. For sample Rh-210, an additional omphacite fraction was separated. Nine to 120 mg of mineral fractions were used for Lu–Hf and Sm–Nd measurements (see Table 3). Prior to digestion, the whole rock powders and mineral separates were spiked with mixed ^{176}Lu-^{180}Hf and ^{149}Sm-^{150}Nd tracers. The digestion procedures employed for whole rocks (bomb digestion) and mineral separates (tabletop digestion) were described in detail by Lagos et al. (2007) and Herwartz et al. (2008). The Lu–Hf separation as well as an additional clean-up step for the Hf fraction was carried out using the method of Münker et al. (2001). Samarium-Nd separation was carried out using the REE-rich matrix cut left over from the Hf separation, using BioRad® AG50W-X8 cation resin (200–400 mesh) and Eichrom Ln-spec resin (Pin and Zalduegui 1997). Procedural blanks were less than 50 pg for both Hf and Nd.

Measurements

Major element whole rock analyses were carried out using a PANalytical ProTrace XRF at Universität Bonn, Germany. The whole rock trace element contents were determined by quadrupole ICPMS using an Agilent 7500cs mass spectrometer at Universität Kiel, Germany. Analytical procedures followed those of Garbe-Schönberg (1993). Lutetium, Hf, Sm and Nd were measured using the Thermo-Finnigan Neptune MC-ICP-MS at the Steinmann-Institut Bonn, operated in static mode. Values of ^{143}Nd/^{144}Nd and ^{176}Hf/^{177}Hf were corrected for mass fractionation using the exponential law and ^{146}Nd/^{144}Nd = 0.7219 and ^{179}Hf/^{177}Hf = 0.7325, respectively. Measured ^{143}Nd/^{144}Nd and ^{176}Hf/^{177}Hf values of the samples are reported relative to ^{143}Nd/^{144}Nd = 0.511859 for the La Jolla Nd standard (measured value = 0.511836 ± 47 (2SE); $n = 2$) and ^{176}Hf/^{177}Hf = 0.282160 for the Münster Ames Hf standard (measured value = 0.282161 ± 44 (2SE); $n = 27$) that is isotopically identical to the JMC-475 standard.

Several garnet grains were also analysed in situ by laser ablation mass spectrometry along line profiles (Fig. 5), in order to measure their Mn and Lu abundances. Laser ablation of these garnet grains was carried out using a Resonetics M50-E ATL Excimer 193 nm laser system coupled to a Thermo-Finnigan X-series 2 quadrupole ICP-MS (Steinmann-Institut Bonn). Spot sizes were set between 33 and 75 μm depending on the size of the garnets analysed, as well as the amount of mineral inclusions found in the cores of the individual grains. Laser fluence at the sample surface was measured at 7 J/cm^{-2}, and the laser repetition rate was set to 15 Hz. Count rates were normalized using ^{29}Si as the internal standard and one external standard (NIST-610 glass, Pearce et al. 1997). The isotopes ^{29}Si, ^{43}Ca, ^{57}Fe, ^{55}Mn and ^{175}Lu were monitored. Data reduction and evaluation were carried out following the procedure laid out by Longerich et al. (1996). Electron microprobe BSE images of the garnets before and after LA-ICP-MS analyses are enclosed in the Electronic Supplementary Material.

Mineral major element abundances were analysed by spot analysis using a JEOL superprobe JXA-8900 microprobe (Universität zu Köln) and a JEOL superprobe JXA-8200 microprobe (Steinmann-Institut Bonn) in wavelength dispersive mode (WDS) employing 15 kV acceleration voltage and 15 nA beam current. Calibrations for Mg, Al, Si, Ti, Ca, Fe, Na, K, Cr and Mn were carried out on andradite, rutile, basaltic glass (VG2–USNM 111240/52), and Jadeite-Diopside synthetic glass. In addition, high-resolution X-ray maps were made for selected garnet grains of all four samples, in order to identify and characterize their zonations with respect to Ca, Fe, Mg and Mn (see Figs. 4, 5). X-ray maps were performed using a JEOL superprobe JXA-8200 microprobe (Steinmann-Institut Bonn), with 15 kV acceleration voltage and 100 nA beam current over 24 h.

Petrography and equilibrium phase diagrams

Mineral compositions of garnet, omphacite, amphibole, phengite, plagioclase and sapphirine were analysed by electron microprobe, the results of which are listed in

Table 1 Compilation of geochronological data of the Rhodope thrust units

	Lower Allochthon	Middle Allochthon	Upper Allochthon
Corresponds to	Pangaion–Pirin complex [1] Thracia terrane [2]	Sidironero-Mesta unit Starcevo unit Asenica unit Madan unit Borovica unit Arda 2 unit	Kimi Complex (Eastern Rhodopes) Vertiskos/Ograzhden unit (SMM) [12] Kardžali unit
Exposure	Metamorphic core complexes South of Nestos Shear zone	North of Nestos Shear zone around core complexes	Eastern Rhodopes around core complexes Western Rhodopes
Lithologies	Composite unit Variscan basement (orthogneisses) metasedimentary sequence	Mixed unit (continental and oceanic) intruded by arc granitoids	Composite unit Metapelites, gneisses, amphibolites Ultramafics (dunites, pyroxenites) Marbles hosting eclogite boudins
Metamorphic grade	Greenschist to amphibolite facies	Up to eclogite facies Locally reaching UHP (microdiamonds)	Eclogite facies Locally reaching UHP (microdiamonds)
Felsic rocks/metapelites			
Inherited components[a]		**3200–500–410–356** [2], [6], [14] **330–250** [2]	**298** [7] **3000–2370–451–290** [7], [10]
Protolith crystallization	**32** [1]; **334–266** [2], [3], [9], [13],	**294** [4], [6]; **170–134** [1], [2], [13]	**151** [10]; **232** [11]; **430** [12]
Metamorphism	Eocene (?) [13]	**Eocene** [4], [6], [1], [13], + **145/148** (?) [14], [6]	**170–160** [7] **82–65** (amphibolite facies ?) [7], [8]
Cooling–uplift–extension	**35–38–56** [3], [9], [13]	**52.8–45–36–32** [4], [13], [15]	**65–62** [8], [5]
Mafic rocks	None reported		
Protolith crystallization		**Min. 77.4 to max. 294 (245–294)** [4], [6] Inherited: **430** [6]	**117.4 (?)** [5]; **288–200** [7]
Metamorphism		**42.2–51** [4], [6]	**160** (HT) [7] **120–115** (HP) [7],[9] **82–73.5** (Low-grade) [7], [5]

Bold values represent recorded age information (in Ma)

[a] Mostly zircon cores in metapelites and gneisses, interpreted to be inherited from sedimentary precursor or from assimilated material

[1] Jahn-Awe et al. (2010); [2] Turpaud and Reischmann (2010); [3] Peytcheva et al. (2004); [4] Liati and Gebauer (1999); [5] Liati et al. (2002); [6] Liati (2005); [7] Bauer et al. (2007); [8] Mposkos and Wawrzenitz (1995); [9] Wawrzenitz and Mposkos (1997); [10] Cornelius (2008); [11] Himmerkus et al. (2009a); [12] Himmerkus et al. (2009b); [13] Ovtcharova et al. (2004); [14] Krenn et al. (2010); [15] Lips et al. (2000)

Tables 4 and 5. Using these data, we calculated equilibrium assemblage diagrams (Fig. 3) for the samples Rh-83, Rh-89 and Rh-210 using the whole rock compositions obtained by XRF (Table 2), the Domino-Theriak program package (de Capitani and Petrakakis 2010) and a modified JUN92 database (Berman 1988; upgrade 1992). The database was modified with non-ideal solid solution models for garnet (Berman 1990), phengite (Massonne and Szpurka 1997), and feldspar (Fuhrman and Lindsley 1988) and ideal approximations for clinopyroxene (endmembers: diopside-hedenbergite-jadeite), clinoamphibole (tremolite, pargasite, Fe-pargasite, glaucophane, tschermakite), spinel (spinel-hercynite), biotite (phlogopite-annite-Mn-biotite), chlorite (chlinochlore-daphnite-Mn-chlorite) and sapphirine. For

Table 2 Major and trace element concentrations of the four studied eclogite samples

Sample ID	Rh-83	Rh-89	Rh-197	Rh-210
Unit	Middle Allochthon	Middle Allochthon	Middle Allochthon	Upper Allochthon
Sub-unit	Starcevo unit	Chepelare suture	Starcevo unit	Kimi Complex
UTM coordinates	E345379 N4606164	E290760 N4620157	E341746 N4601344	E349781 N4578464
Major elements (wt%)				
SiO_2	48.4	47.8	51.1	45.8
Al_2O_3	16.7	15.4	17.0	14.0
Fe_2O_3	10.3	12.4	9.2	14.0
MnO	0.17	0.21	0.18	0.25
MgO	8.32	7.84	6.71	7.43
CaO	10.2	9.34	9.86	12.9
Na_2O	3.35	3.37	4.11	3.14
K_2O	0.47	0.52	0.02	0.02
TiO_2	1.63	2.38	1.18	2.29
P_2O_5	0.15	0.28	0.20	0.17
SO_3	0.41	0.27	0.010	0.27
L.O.I.	0.00	0.19	0.00	0.00
Sum	100.2	100.2	99.6	99.9
Trace elements (ppm)				
Li	8.72	17.2	4.02	17.1
Sc	40.2	37.9	36.0	52.5
V	221	285	203	395
Cr	320	286	264	182
Co	43.4	45.2	32.9	45.6
Ni	94.1	142	54.2	62.0
Cu	35.1	44.7	41.3	74.0
Zn	81.5	106	95.9	103
Ga	17.7	22.8	17.9	18.4
Rb	12.4	15.1	0.986	0.594
Sr	194	151	166	86.6
Y	29.0	47.8	26.5	45.1
Zr	152	200	113	123
Nb	3.37	5.43	5.83	3.54
Mo	0.692	0.858	0.249	0.266
Sn	1.23	2.14	3.07	1.45
Sb	0.0768	0.178	0.0939	0.0487
Cs	0.788	0.464	0.107	0.0176
Ba	94.4	106	6.18	9.36
La	8.57	10.1	19.1	0.894
Ce	22.7	27.4	40.4	3.33
Pr	3.36	4.23	5.22	0.701
Nd	15.7	21.0	21.8	4.73
Sm	4.24	6.34	5.18	2.86
Eu	1.52	2.07	1.58	1.31
Gd	4.91	7.76	5.16	5.61
Tb	0.826	1.33	0.773	1.14
Dy	5.32	8.67	4.70	7.91
Ho	1.10	1.80	0.989	1.69
Er	3.03	4.97	2.86	4.78
Tm	0.445	0.731	0.435	0.719
Yb	2.94	4.81	2.89	4.75
Lu	0.435	0.706	0.432	0.709
Hf	3.42	4.92	2.82	3.24
Ta	0.232	0.371	0.381	0.264
W	0.209	0.545	0.461	0.355
Tl	0.174	0.154	0.0201	0.024
Pb	2.63	1.94	5.32	0.727
Th	0.585	0.927	4.01	0.0573
U	0.132	0.195	0.914	0.194

Table 3 Lu-Hf and Sm–Nd isotope compositions of the whole rocks and mineral separates

Sample ID		Weight (mg)	ppm Lu	ppm Hf	$^{176}Lu/^{177}Hf \pm 2\sigma$	$^{176}Hf/^{177}Hf \pm 2\sigma$	ppm Sm	ppm Nd	$^{147}Sm/^{144}Nd \pm 2\sigma$	$^{143}Nd/^{144}Nd \pm 2\sigma$
Rh-83	*Whole rock*	80.3	0.437	3.39	0.01830 ± 6	0.282918 ± 6	3.79	13.9	0.1645 ± 3	0.512759 ± 17
Rh-83_Gt-1	*Garnet*	80.9	1.75	0.117	2.126 ± 7	0.284670 ± 35				
Rh-83_Gt-2	*Garnet*	34.1	1.91	0.119	2.280 ± 7	0.284768 ± 23				
Rh-83_Gt-3	*Garnet*	52.8	1.69	0.150	1.599 ± 5	0.284251 ± 17				
Rh-83_Gt-4	*Garnet*	12.7	1.82	0.0906	2.853 ± 9	0.285340 ± 76				
Rh-83_Gt-5	*Garnet*	9.85	1.81	0.0889	2.892 ± 11	0.285396 ± 78				
Rh-89	*Whole rock*	79.8	0.713	4.78	0.02118 ± 7	0.283017 ± 4	5.98	20.1	0.1799 ± 4	0.512863 ± 12
Rh-89_Gt-1	*Garnet*	119	1.89	0.0789	3.398 ± 11	0.285765 ± 17				
Rh-89_Gt-2	*Garnet*	47.2	1.90	0.0904	2.993 ± 9	0.285418 ± 30				
Rh-89_Gt-3	*Garnet*	62.4	1.87	0.107	2.470 ± 8	0.284998 ± 19				
Rh-197	*Whole rock*	81.1	0.432	2.92	0.02096 ± 7	0.282821 ± 6	4.71	20.0	0.1425 ± 3	0.512514 ± 15
Rh-197_Gt-1	*Garnet*	92.2	1.59	0.0599	3.779 ± 12	0.285830 ± 23				
Rh-197_Gt-2	*Garnet*	52.0	1.65	0.0624	3.760 ± 12	0.285802 ± 29				
Rh-197_Gt-3	*Garnet*	50.4	1.70	0.0688	3.519 ± 11	0.285611 ± 27				
Rh-197_Gt-4	*Garnet*	32.9	1.66	0.0567	4.151 ± 13	0.286096 ± 72				
Rh-210	*Whole rock*	80.1	0.714	2.92	0.03468 ± 11	0.283098 ± 6	2.60	4.3	0.3664 ± 7	0.513129 ± 23
Rh-210_Gt-1	*Garnet*	108	1.82	0.0854	3.029 ± 9	0.290157 ± 11				
Rh-210_Gt-2	*Garnet*	63.6	1.89	0.0799	3.368 ± 10	0.290960 ± 17				
Rh-210_Gt-3	*Garnet*	67.5	1.80	0.104	2.448 ± 8	0.288735 ± 16				
Rh-210_Gt-4	*Garnet*	50.8	1.83	0.0863	3.016 ± 9	0.290099 ± 25	2.35	1.96	0.7261 ± 15	0.513389 ± 20
Rh-210_Px-1	*Pyroxene*	47.3	0.00964	1.10	0.001245 ± 7	0.283011 ± 19	1.22	1.67	0.4400 ± 9	0.513193 ± 20

Table 4 Representative microprobe analyses of eclogite phases in weight % and p.f.u.

	Rh-83 Grt Core	Rh-83 Grt Rim	Rh-83 Omp1	Rh-83 Omp2 Sympl	Rh-83 Amp	Rh-197 Grt Core	Rh-197 Grt Rim	Rh-197 Cpx	Rh-197 Amp	Rh-89 Grt Core	Rh-89 Grt Rim	Rh-89 Omp	Rh-89 Cpx	Rh-89 Amp	Rh-89 Phengite	Rh-210 Grt Core	Rh-210 Grt Rim	Rh-210 Omp	Rh-210 Amp	Rh-210 Phengite
SiO_2	39.9	39.5	55.0	53.1	39.0	38.6	40.0	54.9	39.9	39.0	38.3	54.2	52.4	42.0	52.8	39.6	39.7	54.6	43.9	50.7
TiO_2	0.03	0.03	0.09	0.27	0.56	0.09	0.01	0.04	1.71	0.09	0.03	0.10	0.35	0.67	0.70	0.01	0.07	0.21	0.55	1.44
Al_2O_3	22.4	22.0	11.2	8.0	17.8	21.1	22.7	1.4	17.7	21.3	21.2	10.4	4.7	13.8	26.6	21.9	22.4	9.82	16.1	28.0
FeO	21.2	22.8	3.37	5.12	12.7	22.2	23.6	8.26	10.3	23.1	23.9	5.58	4.76	11.2	1.30	20.4	20.5	6.69	11.6	2.48
MnO	0.65	0.26	–	0.09	0.08	4.20	0.65	0.05	0.06	0.59	0.39	0.04	0.01	0.06	–	1.50	0.46	0.07	0.04	–
MgO	9.43	7.89	9.67	11.9	12.1	3.08	8.77	14.2	12.8	8.46	9.57	9.50	13.8	14.4	3.95	4.96	6.63	8.72	11.7	3.33
CaO	7.22	8.31	14.4	18.6	10.4	11.1	6.71	21.0	10.9	7.86	5.69	15.7	20.9	11.4	–	11.8	10.2	14.7	9.64	0.02
Na_2O	–	–	6.45	3.55	3.25	0.03	–	2.14	3.29	–	0.01	5.38	2.70	3.09	0.51	0.04	0.01	6.23	4.13	0.40
K_2O	0.02	–	0.01	–	0.69	–	0.01	0.01	0.20	–	–	0.01	0.01	0.71	10.2	0.01	0.01	0.02	0.15	10.1
Cr_2O_3	0.04	0.01	–	0.02	0.04	0.08	–	0.05	0.04	–	0.04	0.02	0.06	0.08	–	–	0.03	0.04	0.01	–
Total	100.9	100.8	100.1	100.6	96.6	100.5	102.5	102.0	96.9	100.4	99.1	100.9	99.7	97.5	96.1	100.2	100.1	101.1	97.9	96.4
Si	6.01	6.00	1.96	1.92	5.83	6.04	5.97	2.00	5.87	5.97	5.94	1.94	1.93	6.19	3.47	6.08	6.05	1.96	6.37	3.34
Ti	–	–	–	0.01	0.06	0.01	–	–	0.19	0.01	–	–	0.01	0.07	0.03	–	0.01	0.01	0.06	0.07
Al	3.94	3.97	0.47	0.34	3.14	3.90	4.00	0.06	3.07	3.85	3.87	0.44	0.20	2.40	2.06	3.97	4.02	0.42	2.74	2.17
Fe	2.90	2.66	0.10	0.15	1.59	2.91	2.95	0.25	1.26	2.96	3.10	0.17	0.15	1.38	0.07	2.62	2.61	0.20	1.41	0.14
Mn	0.03	0.08	–	–	0.01	0.56	0.08	–	0.01	0.08	0.05	–	–	0.01	–	0.19	0.06	–	0.01	–
Mg	1.79	2.11	0.51	0.64	2.71	0.72	1.95	0.77	2.81	1.93	2.21	0.51	0.75	3.16	0.39	1.13	1.51	0.47	2.53	0.33
Ca	1.35	1.16	0.55	0.72	1.66	1.86	1.07	0.82	1.71	1.29	0.95	0.60	0.82	1.80	–	1.94	1.67	0.56	1.50	–
Na	–	–	0.45	0.25	0.94	0.01	–	0.15	0.94	–	–	0.37	0.19	0.88	0.065	0.01	–	0.43	1.16	0.05
K	–	0.003	–	–	0.13	0.001	0.002	–	0.04	0.001	–	–	–	0.13	0.86	–	–	–	0.03	0.85
Cr	–	0.01	–	–	–	0.01	–	–	–	–	–	–	–	–	–	–	–	–	–	–
Total	16.0	16.0	4.03	4.03	16.1	16.0	16.0	4.05	15.9	16.1	16.1	4.03	4.06	16.0	6.93	15.9	15.9	4.05	15.8	6.95
O	24	24	6	6	23	24	24	6	23	24	24	6	6	23	11	24	24	6	23	11

All Fe is calculated as Fe^{2+}

See also Table 5

Table 5 Representative microprobe analyses of phases observed in Al-rich coronae in weight% and p.f.u

	Rh-83 Spr Sympl. core	Rh-83 Spl Sympl. core	Rh-83 Pl Sympl. core	Rh-83 Pl Sympl. rim	Rh-197 Grt Core	Rh-197 Amphibole	Rh-197 Spl Sympl. core	Rh-197 Ilm Sympl. core	Rh-197 Pl Sympl. core	Rh-197 Pl Sympl. rim
Proportion in corona [%]	*8*	*30*	*60*			*13.5*	*4.5*	*2*	*48*	
SiO_2	10.7	0.04	57.5	64.1	38.6	39.9	0.05	0.53	55.7	61.7
TiO_2	0.02	0.05	0.01	0.04	0.09	1.71	0.08	44.8	0.00	0.03
Al_2O_3	69.7	66.3	27.6	23.2	21.1	17.7	61.2	0.16	27.8	23.4
FeO	3.94	16.2	0.19	0.09	22.2	10.3	23.7	43.7	0.12	0.14
MnO	0.06	0.08	0.03	0.00	4.20	0.06	0.06	0.46	0.02	0.00
MgO	16.2	17.0	0.04	0.00	3.08	12.8	11.3	0.45	0.01	0.00
CaO	0.19	0.08	9.01	4.09	11.1	10.9	0.11	0.22	9.37	4.53
Na_2O	0.09	0.00	6.37	8.68	0.03	3.29	0.00	0.08	5.94	8.72
K_2O	0.00	0.00	0.08	0.19	0.00	0.20	0.00	0.02	0.02	0.06
Cr_2O_3	0.09	0.12	0.01	0.00	0.08	0.04	0.18	0.04	0.02	0.03
Total	101.0	99.8	100.9	100.3	100.5	96.9	96.6	90.5	99.0	98.6
Si	1.25	0.00	2.56	2.81	6.04	5.87	0.00	0.02	2.52	2.77
Ti	0.00	0.00	0.00	0.00	0.01	0.19	0.00	0.95	0.00	0.00
Al	9.58	2.00	1.45	1.20	3.90	3.07	1.99	0.01	1.49	1.24
Fe	0.35	0.35	0.01	0.00	2.91	1.26	0.55	1.03	0.01	0.01
Mn	0.01	0.00	0.00	0.00	0.56	0.01	0.00	0.01	0.00	0.00
Mg	2.82	0.65	0.00	0.00	0.72	2.81	0.46	0.02	0.00	0.00
Ca	0.02	0.00	0.43	0.19	1.86	1.71	0.00	0.01	0.46	0.22
Na	0.02	0.00	0.55	0.74	0.01	0.94	0.00	0.00	0.52	0.76
K	0.00	0.00	0.00	0.01	0.00	0.04	0.00	0.00	0.00	0.00
Cr	0.01	0.00	0.00	0.00	0.01	0.00	0.00	0.00	0.00	0.00
Total	14.1	3.00	5.00	4.96	16.0	15.9	3.00	2.04	4.99	4.99
O	20	4	8	8	24	23	4	3	8	8

	Rh-83 Corona	Rh-197 Corona
Si	26.9	38.6
Ti	1.81[a]	0.94
Al	46.4	43.8
Fe	4.72	3.05
Mn	0	0
Mg	10.1	3.18
Ca	4.42	5.24
Na	5.62	5.17
K	0	0
Cr	0	0
H	0	1.70[b]
Total	100	101.7
O	149.1	159.7

Estimated compositions of the coronae are used as input for calculation of equilibrium assemblage diagrams

[a] 2% TiO_2 (Rutile) added to corona composition

[b] Assuming 2OH for the amphibole

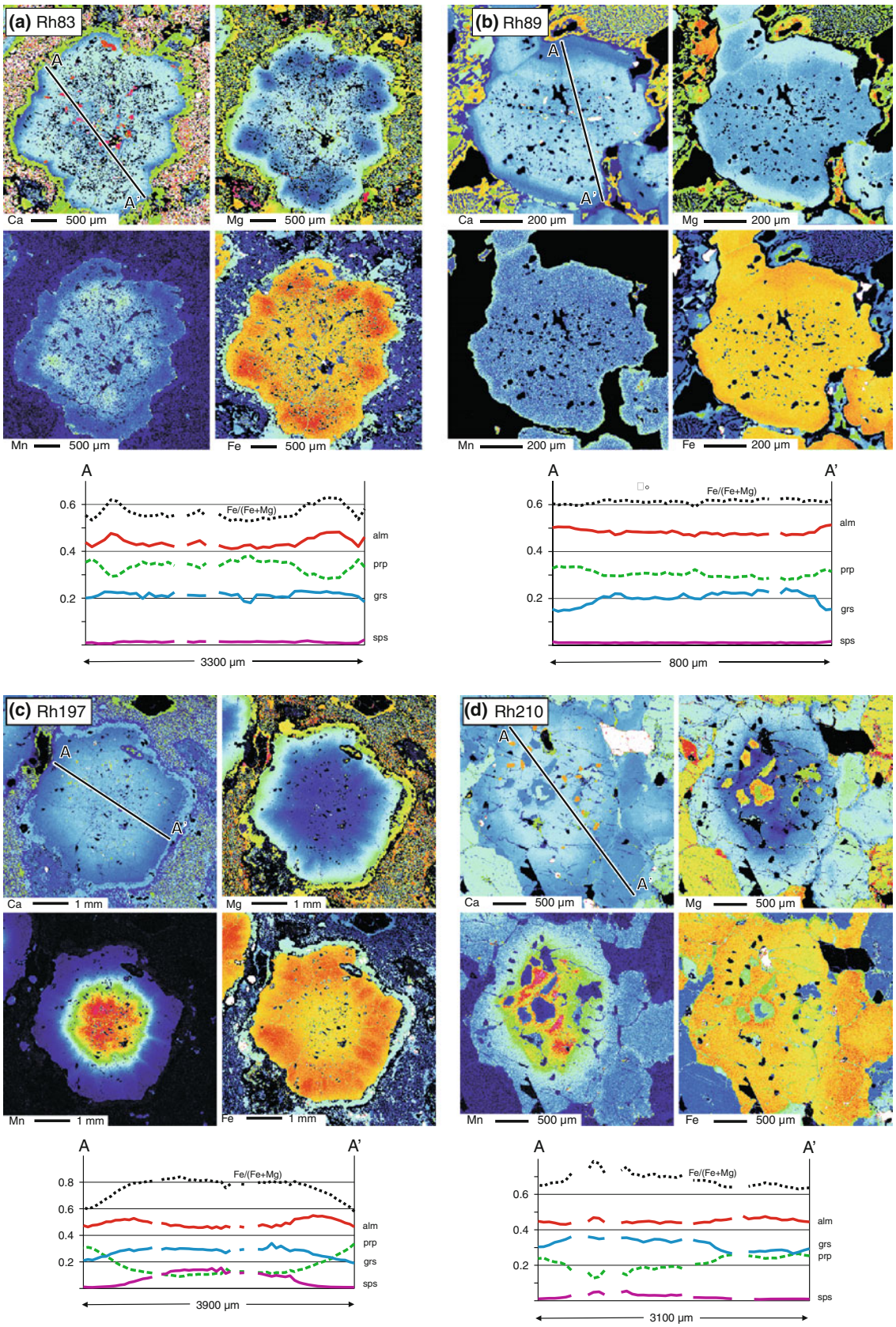

Fig. 4 **a–d** Major element distribution maps and cross-sections through representative garnets from the four eclogite samples obtained by electron microprobe analyses

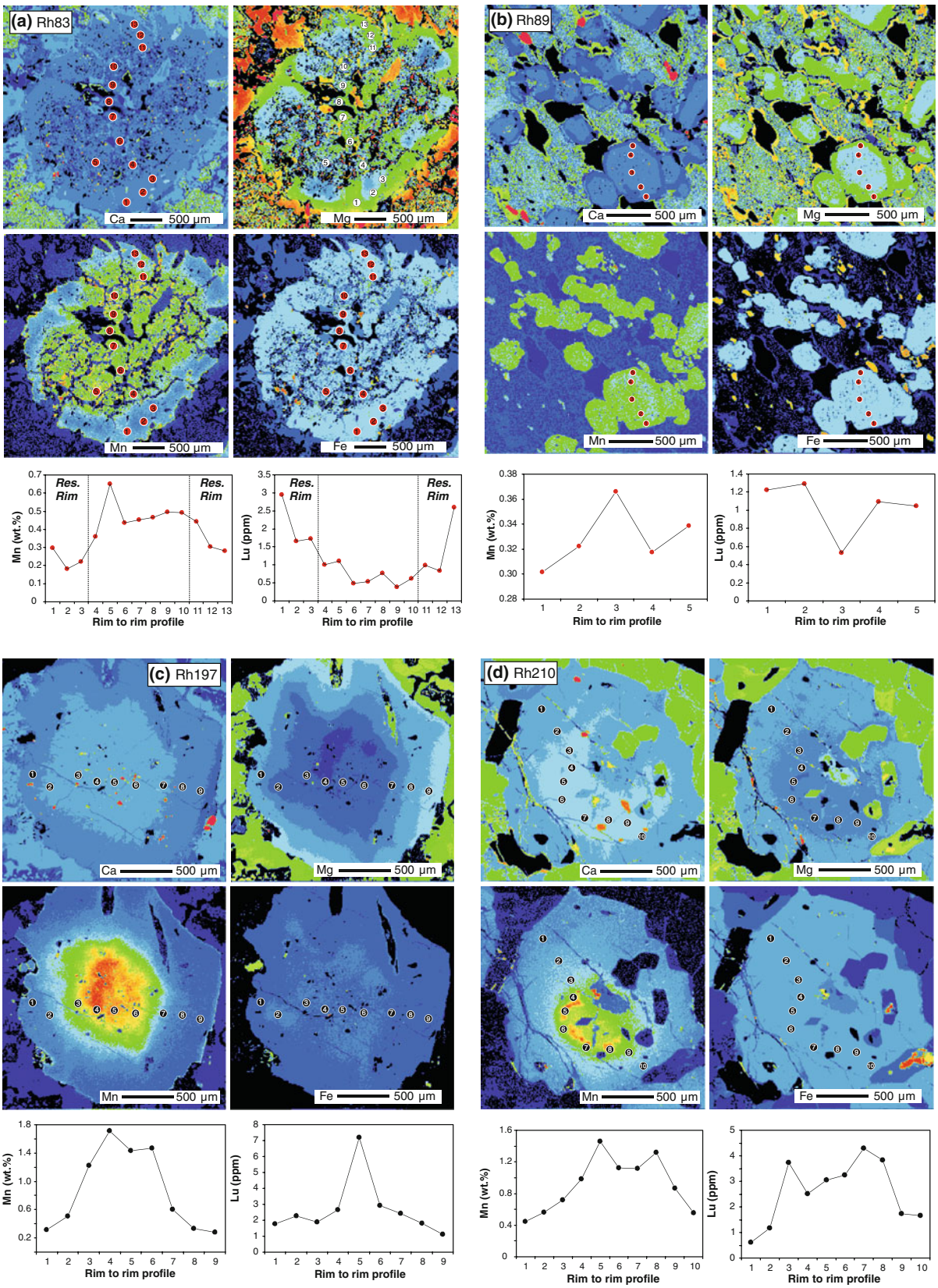

Fig. 5 **a–d** Major element distribution map of the garnets analysed by LA-ICP-MS as well as the element profiles obtained by LA-ICP-MS for Lu and Mn. BSE images of the selected garnet grains before and after laser ablation are enclosed in the Electronic Supplementary Material. Note that "Res. Rim" in the Lu and Mn profiles of **c** corresponds to resorbed garnet rim domains

sapphirine, we chose Mg-sapphirine $Mg_{3.5}AL_9Si_{1.5}O_{20}$ and Fe-sapphirine $Fe_{3.5}AL_9Si_{1.5}O_{20}$ as end-members, as these are compositionally close to the sapphirine observed in sample Rh-83. ΔfH_0 and S_0 of the sapphirine and daphnite end-members were adopted from Holland and Powell (1998) and slightly adjusted so that the internal consistency of the database was maintained. The equilibrium assemblage diagrams were calculated for water-saturated Si–Al-Ti–Fe–Mn–Mg-Ca–Na–K bulk rock compositions (see Table 2). In order to constrain the retrograde P–T path, we also calculated one diagram in a Si–Al-Ti–Fe–Mn–Mg-Ca–Na–K system for a retrograde corona forming around decomposing kyanite (sample Rh-83). The composition was estimated from the proportions and compositions of the minerals constituting the coronae (see Table 5).

Sample Rh-83 from the Middle Allochthon (Starcevo Unit) is a sapphirine-bearing kyanite eclogite, from the same unit as and similar to those described by Kolčeva et al. (1986) and Liati and Seidel (1996). It contains the high-pressure assemblage garnet-omphacite1 ($Jd_{37–43}$)-kyanite-quartz-rutile-zoisite-apatite, corresponding to 600-830°C/19–27.5 kbar in the equilibrium assemblage diagram (Fig. 3a). Phengite was not observed, probably because it was completely consumed during retrograde growth of amphibole and biotite. Most of the omphacite was replaced during several stages of retrograde overprint, starting with the growth of pargasitic amphibole (mostly around garnet) and omphacite2 ($Jd_{17–26}$)-plagioclase symplectites (mostly at the expense of omphacite1) that show ambiguous textural relations with the pargasitic hornblende. Symplectites of plagioclase ($Ab_{29–57}An_{41–69}$), spinel and sometimes rutile, sapphirine and/or corundum formed around decomposing kyanite (see BSE images in the Electronic Supplementary Material). Biotite is locally pseudomorphic after amphibole and together with plagioclase forms patches after the sapphirine-bearing symplectite coronae. Garnets in Rh-83 are several millimetre large, corroded grains that display a complex chemical zonation (Fig. 4a). A wide rim domain displays patches enriched in Fe and Ca and depleted in Mg. The inclusion-rich core has a composition similar to the outermost rim with respect to Fe, Mg and Ca, but shows a higher Mn content than the rest of the grain. This Mn-rich domain preserves an edgy euhedral shape in some garnet grains (Fig. 4a) and a more diffuse shape in others (Fig. 5a). We interpret this compositional pattern to result from partial resetting (resorption) of the garnet rims that also result in an increase in abundance of trace elements like Lu in the resorbed rims (Fig. 5a and discussion below).

Based on chemical and textural evidence, we propose that the growth of the plagioclase-spinel-sapphirine symplectites around kyanite was controlled by local chemical equilibria. Therefore, we used a composition estimated as described above (Table 5) as input for the calculation of the equilibrium assemblage diagram (Fig. 3b). For a dry composition, the observed assemblage plagioclase-spinel-sapphirine-corundum-rutile is predicted to be stable in the grey-shaded field of Fig. 3b, that is, above 610°C. Adding excess water to the same composition leads to a shift of the plagioclase-spinel-sapphirine-corundum-rutile stability field to higher temperatures, that is, above 670°C. The maximum pressure is constrained by the boundary of the plagioclase-spinel-sapphirine-corundum-rutile stability field towards garnet stability and increases from c. 8 kbar at 710°C to c. 12.5 kbar at 900°C. It is therefore realistic to assume that the sapphirine-bearing coronae formed at temperatures around or even below 700°C, that is, roughly at the same temperatures where the orthogneissic country rocks underwent migmatization (Georgieva et al. 2002). Likewise, if calculated for a broader compositional range, the absence of garnet from the observed assemblage requires pressures significantly below those of a high-pressure granulite-facies overprint above 12 kbar, which was previously postulated by various authors (Liati and Seidel 1996, Carrigan et al. 2002).

The matrix assemblage of sample Rh-197 (Starcevo Unit) is much more strongly affected by retrogression than documented for sample Rh-83. However, large garnet porphyroblasts are much better preserved, are euhedral and clearly exhibit growth zonation (Figs. 4c, 5c). Manganese, Ca and the Fe to (Fe+Mg) ratio show the classic bell-shaped distribution. Zonations of Fe and particularly Mn are edgy, discontinuous and parallel to the grain boundaries. Nevertheless, garnets in Rh-197 also display thin channels, along which transport and some re-equilibration might have occurred (Fig. 4c). However, Lu element profiles (Fig. 5c) strongly indicate that garnets in Rh-197 preserve their original trace element zonation displayed by the high Lu concentration in the core and decreasing concentrations towards the rims (see also discussion below). Clinopyroxene ($Di_{62–79}Hd_{6–23}Acm_{5–15}Jd_{1–4}$) is abundant in symplectites with plagioclase. Pargasitic amphibole grew along the rims of garnet and within the matrix. Rh-197 also contains Al-rich symplectite patches comprising plagioclase ($Ab_{46–57}An_{43–53}$), kyanite, amphibole, spinel, ilmenite and sometimes corundum (see BSE images in the Electronic Supplementary Material). Unlike in Rh-83, we did not observe specific mineral relicts within the symplectite patches.

Sample Rh-89 contains the high-pressure assemblage garnet-omphacite ($Jd_{27–35}$)-quartz-phengite-rutile, corresponding to the grey-shaded stability field in the phase diagram (Fig. 3c). Garnets occur as slightly corroded, euhedral grains and are much smaller than in the two previous samples (Figs. 4b, 5b). They show distinct Ca-poor and Fe- and Mg-rich rims. The Fe to (Fe+Mg) ratio

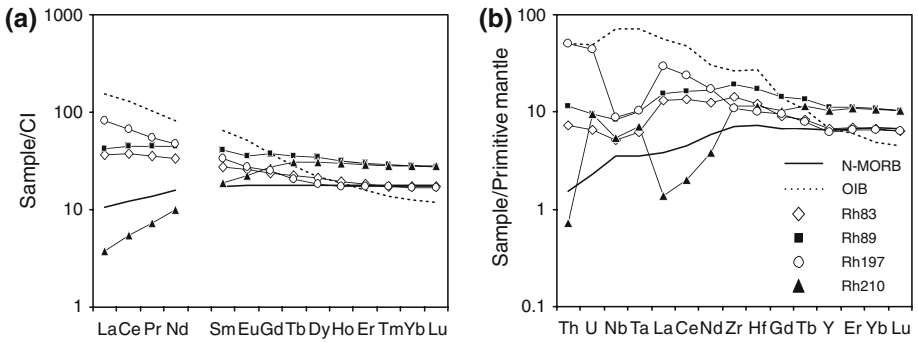

Fig. 6 Trace element composition of the four eclogite samples studied. **a** CI-normalized trace element pattern of the four eclogite samples as well as OIB and N-MORB (after Sun and McDonough 1989). **b** Primitive mantle-normalized multi-element diagram of the four eclogite samples along with values for OIB and N-MORB for comparison (after Sun and McDonough 1989)

Fig. 7 Lu-Hf isochrons for the four eclogite samples and a Sm–Nd isochron of sample Rh-210 from the Upper Allochthon. The elevated errors on sample splits Rh-83 Gt-4 and Gt-5 as well as Rh-197 Gt-4 reflect the smaller amount of analysed Hf in these splits (see also Table 3)

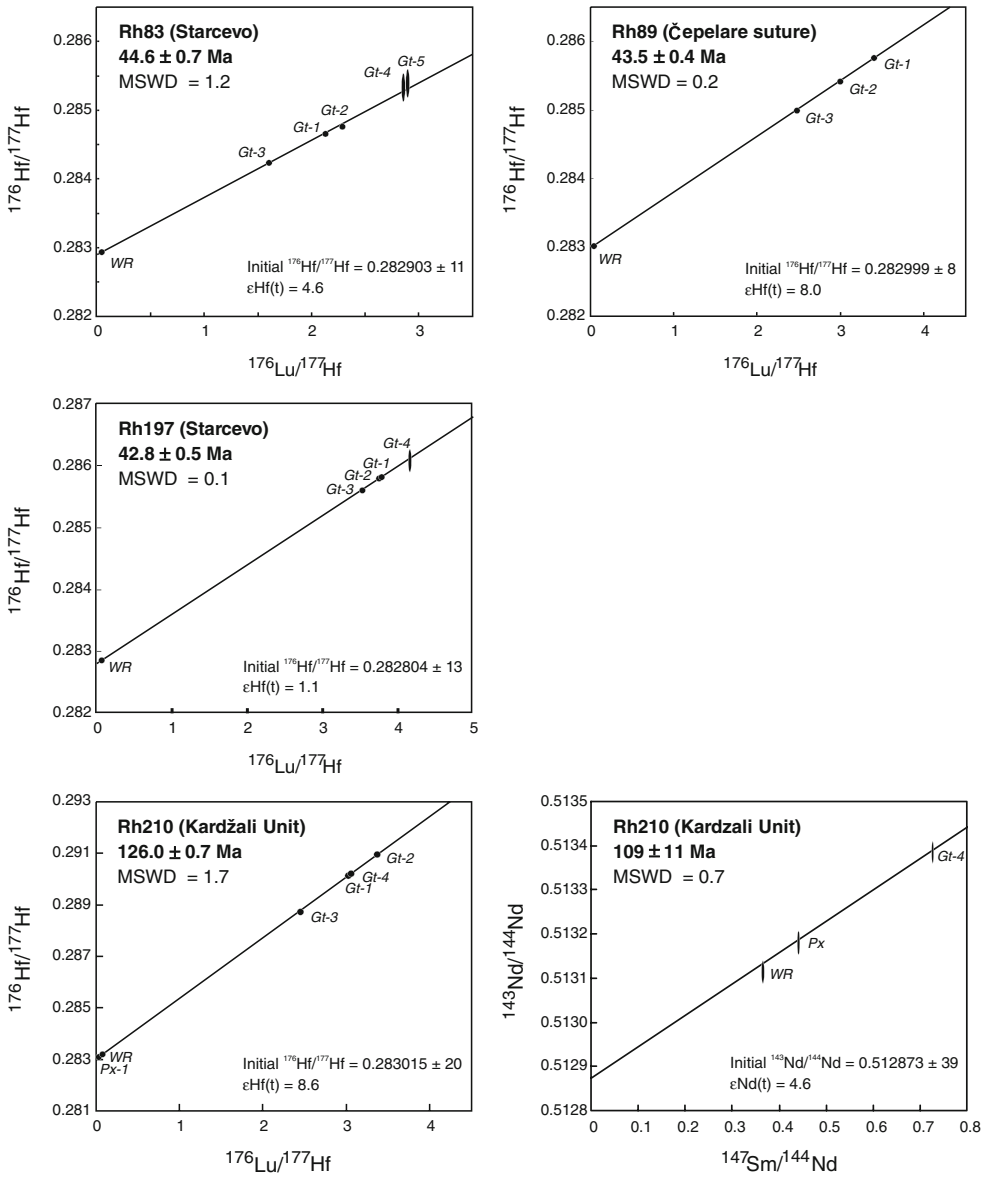

is slightly elevated in the core. However, the distribution of Mn is flat (Figs. 4b, 5b) and indicates resorption of garnet. Altogether, the chemical zoning, at least of Fe, Mg and Mn, appears to be strongly reset in sample Rh-89, which is also documented by the enrichment of Lu in the rim domains (Fig. 5b). Metamorphic retrogression caused growth of pargasitic amphibole, plagioclase-clinopyroxene ($Di_{70–83}Hd_{0–18}Acm_{0–12}Jd_{8–12}$) symplectites and biotite together with plagioclase. Al-rich symplectites as in Rh-83 and Rh-197 were not observed in Rh-89.

The overlapping stability fields of the high-pressure assemblages in samples Rh-83 and Rh-89 and the Al-rich symplectites in both Rh-83 and Rh-197 allow to roughly constrain a pressure–temperature path for the exhumation of the lower part of the Middle Allochthon (Fig. 3d).

The observed high-pressure assemblage in Rh-210 is garnet-omphacite ($Jd_{32–41}$)-amphibole-phengite-rutile. Mica is scarce (<1%) due to the low potassium content of the sample (0.02 wt%). Garnets are again large (>2 mm) and show original growth zonation with humps of Ca, Mn and the Fe to (Fe+Mg) ratio (Fig. 4d) and Lu (Fig. 5c) in the core. In the equilibrium assemblage diagram (Fig. 3e), this assemblage is predicted to be stable under somewhat lower pressures (15–19 kbar) than those estimated from the high-pressure assemblages of the samples from the Middle Allochthon (20–25 kbar). Sample Rh-210 exhibits little evidence of retrogression other than the growth of chlorite along isolated cracks.

Geochemical results

Major and trace elements

The major and trace element concentrations of all four eclogite samples are given in Table 2. The four analysed samples yield basaltic whole rock compositions (SiO_2 = 45.8–51.1 wt. %; MgO = 6.71–8.32 wt. %; Al_2O_3 = 14.0–17.0 wt. %), with both high Zr (113–200 ppm) and compatible element contents (e.g., Cr = 182–320 ppm; Ni = 54.2–142 ppm).

With the exception of sample Rh-210, all samples are LREE-enriched (La_N/Yb_N = 1.4, 2.0, 4.5 for Rh-83, Rh-89 and Rh-197, respectively), but exhibit similar magnitudes of HREE abundances as N-MORB (Fig. 6a). Sample Rh-210 from the Upper Allochthon is characterized by a strong LREE depletion and a slight enrichment of the HREE with respect to N-MORB (La_N/Yb_N = 0.13). In the primitive mantle-normalized trace element diagram (Fig. 6b), sample Rh-210 is depleted in Th and La, Ce and Nd and displays positive anomalies of high field strength elements (HFSE) like Nb, Ta, Zr and Hf. In contrast, sample Rh-197 displays a striking negative Nb–Ta anomaly and Th-U enrichment. Samples Rh-83 and Rh-89 are enriched with respect to N-MORB (Fig. 6b), especially with regard to U and Th. All four samples display similar Nb/Ta ranging from 13.4 to 15.3 at high Zr/Hf (37.9–44.5), broadly overlapping the range of values found in MORBs and island-arc basalts (Büchl et al. 2002; Münker et al. 2004).

Lu–Hf and Sm–Nd geochronology

We analysed the four eclogite samples for their Lu–Hf and Sm–Nd isotope compositions, using one whole rock aliquot as well as three to five mineral separates per sample (garnets and pyroxenes).

The results of the Lu–Hf and Sm–Nd measurements are given in Table 3 and are illustrated in Fig. 7. Isochron regressions were calculated using ISOPLOT v.2.49 (Ludwig 2001) and $\lambda\ ^{176}Lu = 1.867 \times 10^{-11}$ year^{-1} (Scherer et al. 2001; Söderlund et al. 2004). The external reproducibilities of the isochron calculations were estimated by the empirical relationship 2σ external reproducibility $\approx 4\sigma_m$ (σ_m = standard error of a single analysis; Bizzarro et al. 2003).

The Hf contents of the whole rock samples range from 2.92 to 4.78 ppm and those of the garnets from 60 to 150 ppb. The $^{176}Lu/^{177}Hf$ of the garnets range from 1.60 to 3.78 and the pyroxenes from sample Rh-210 display a $^{176}Lu/^{177}Hf$ of 0.00124. For each sample, mineral separates and whole rock aliquots define statistically significant isochrons (MSWDs of 0.1–0.7; Fig. 7), also suggesting full sample-spike equilibrium during tabletop digestion. The Lu–Hf ages of the samples from the Middle Allochthon are 44.6 ± 0.7 Ma for Rh-83 (n = 6), 43.5 ± 0.4 Ma for Rh-89 (n = 4) and 42.8 ± 0.5 Ma for Rh-197 (n = 5). The sample from the Upper Allochthon (Rh-210) yields a Lu–Hf age of 126.0 ± 0.7 Ma (n = 6).

The Nd contents of the whole rock samples range from 4.28 to 20.1 ppm with $^{147}Sm/^{144}Nd$ of 0.14–0.37. The garnet (Gt-4) and the pyroxene (Px-1) fractions of sample Rh-210 display Nd concentrations of 1.96 and 1.67 ppm with $^{147}Sm/^{144}Nd$ of 0.726 and 0.440, respectively. The Sm–Nd age determined for sample Rh-210 is 109 ± 11 Ma (n = 3). Samarium-Nd garnet analyses of the other three samples were hampered by the presence of inclusions with low Sm/Nd in garnet.

Discussion

Significance of the Lu–Hf geochronological results

In order to adequately interpret the age information from the analysed garnet populations, several important issues have to be addressed first. Two major points addressed here

in detail are the representative sampling of garnet as well as protracted metamorphism and garnet growth.

Representative sampling of bulk garnet and the problem of inclusions

The mineral separation technique employed in this study allows to test for any possible bias in the analysed garnet separates. Pure garnet fractions (without visible inclusions; Gt-1, Gt-4, Gt-5 of each sample) as well as garnet fractions with a high density of inclusions were separated (Gt-2, Gt-3; see also Figs. 4 and 5, garnet major element distribution maps) and used for the Lu–Hf/Sm–Nd geochronological study. As illustrated in Fig. 7, all garnet separates define isochrons with considerably low MSWDs (<1.7).

Furthermore, inclusions in garnet may significantly compromise the measured Hf isotope composition (e.g., Scherer et al. 2000). This issue is readily avoided by the employed tabletop digestion technique, which prevents the dissolution of Hf-rich phases like rutile or zircon (e.g., Scherer et al. 2000; Lagos et al. 2007). In contrast to the Lu–Hf isotope system, the Sm–Nd system is very sensitive to inclusions of apatite and monazite (Scherer et al. 2000) that are abundant as inclusions in garnet in samples Rh-83, Rh-89 and Rh-197, lowering the $^{147}Sm/^{144}Nd$ of the garnet separates. Hence, no meaningful Sm–Nd age could be determined for the samples from the Middle Allochthon.

Constraints on protracted metamorphism and garnet growth

The good fit of all isochrons (MSWDs $\leq$ 1.7) strongly suggests that the Lu–Hf isotope system was not disturbed at a later stage, that is, that garnets and whole rocks remained closed systems after formation. This is especially interesting for sample Rh-210 from the Upper Allochthon, which yields a Lu–Hf age of 126 $\pm$ 0.7 Ma. Based on U–Pb geochronology on zircons, Bauer et al. (2007) and Liati et al. (2002) infer a metamorphic event at ca. 74–77 Ma for the Kimi Complex, which supposedly reached amphibolite-facies conditions (Bauer et al. 2007) or even eclogite- to UHP metamorphic conditions (Liati et al. 2002). Considering the results of the Lu–Hf and Sm–Nd geochronology of sample Rh-210 as well as similar results by Wawrzenitz and Mposkos (1997; 117 $\pm$ 3.5 Ma; Sm–Nd of gt-cpx-whole rock of a garnet-pyroxenite), it appears rather unlikely that a high-grade (eclogite- or UHP) post-Barremian metamorphic event affected sample Rh-210. To a certain degree, similar conclusions can be drawn with regard to older metamorphic events affecting the rocks from the Middle Allochthon as suggested from U–Pb zircon geochronology ($\sim$148 Ma, for the Nestos Shear Zone; Liati 2005; Krenn et al. 2010). If garnet relicts from this Late Jurassic high-grade event had been preserved in the studied eclogite samples, then a mixture of old (radiogenic $^{176}Hf/^{177}Hf$; = garnet cores) and young (unradiogenic $^{176}Hf/^{177}Hf$; = garnet rims) garnet domains would be expected. Such observations have recently been made by Herwartz et al. (2011) for the Adula Nappe in the Central Alps.

Consequently, the Lu–Hf isochrons defined by the studied Rhodopean eclogites argue either (1) for a pervasive nature of both the Eocene and Cretaceous HP events in the Starcevo Unit and the Kardžali Unit, respectively or (2) for the absence of relictic garnet associated with previous metamorphic events in the respective unit. Moreover, the low MSWDs and the generally good fit between three (Rh-83, Rh-89 and Rh-197) of the four Lu–Hf isochrons provide strong evidence for a relatively short duration of garnet growth during the Eocene metamorphic cycle. This is also in line with the phase diagrams (Fig. 3) that predict garnet growth over a relatively small P–T interval just before reaching peak pressure conditions, that is, only above 500°C. If garnet grew over a period of several tens of Myr, the data points would show a higher scatter, that is., a higher MSWD (e.g., Kohn 2009).

Prograde growth ages versus cooling ages

During the nucleation and subsequent growth of garnets along a prograde P–T path, minerals such as garnet develop a growth zonation, which can be approximated by a Rayleigh process (or fractional crystallization and thermodynamic equilibrium; after Kohn 2003). Of fundamental interest here is the preservation of undisturbed distribution patterns for Lu–Hf (and Sm–Nd) in the garnets. Especially during the thermal peak of metamorphism diffusion of these elements would get enhanced. These effects may reset the Lu–Hf and Sm–Nd isotope systems, and the ages defined by the isochrons may then reflect cooling ages. Element diffusivity in garnet depends on a variety of other factors in addition to temperature, for example, grain size, peak temperature, garnet composition, matrix composition, oxygen fugacity (f_2), duration of prograde metamorphism, cooling rate and ionic charge (e.g., Chakraborty and Rubie 1996; Ganguly et al. 1998; van Orman et al. 2002; Skora et al. 2006, Caddick et al. 2010). A useful proxy to assess the effects of diffusion is the major element zonation found in garnets (Figs. 4, 5). As shown by experimental studies (e.g., van Orman et al. 2002), the ionic charge of an element exerts a major control on its diffusivity, where 2+ ions diffuse by orders of magnitude faster than 3+ (e.g., Lu), and presumably 4+ ions (e.g., Hf). Furthermore, it appears that the Lu–Hf system is more resistant to diffusion compared to the Sm–Nd system, as relatively higher

closure temperatures have been proposed for Lu–Hf (e.g., Scherer et al. 2000; Lapen et al. 2003).

The bell-shaped distributions of Mn, Ca and Fe/(Fe+Mg) in garnet in combination with elevated Lu concentrations in the garnet cores as it is shown for samples Rh-197 (Figs. 4c, 5c) and Rh-210 (Figs. 4d, 5d) can therefore be readily regarded as evidence for the preservation of the prograde growth zonation patterns for Lu–Hf. In these two cases, the Lu–Hf ages clearly reflect the time of garnet growth (e.g., Lapen et al. 2003). Based on mass balance arguments, however, Skora et al. (2009) pointed, furthermore, out that the Lu–Hf ages reflect peak metamorphic conditions due to volumetrically higher abundance of garnet rims relative to garnet cores.

The large garnets in sample Rh-83 show a certain degree of garnet rim resorption (~30% of the garnet radius). However, the very cores still show elevated Mn (and to a certain degree also Lu) contents. Considering the near-identical Lu–Hf age of Rh-83 (44.6 ± 0.7 Ma) with that of Rh-197 (42.8 ± 0.5 Ma), it is evident that resorption of the garnet rims is geochronologically barely resolvable and must have occurred at near-peak metamorphic conditions. Otherwise, the Lu that diffused back into the garnet rims would have compromised the fit of the Lu–Hf isochron and biased the isochron towards an apparently younger age (see Kelly et al. 2011).

The more or less homogeneous major element composition of the small garnets in sample Rh-89 (Figs. 4b, 5b) probably results from diffusive reequilibration of formerly prograde zoned garnets. However, this feature may not necessarily indicate a concurrent diffusive mobilization of REEs, in line with findings by Dutch and Hand (2010), who reported garnets with flat equilibrated major element zonations but preserved primary REE zonations. Major element distribution maps shown in Figs. 4b and 5b in combination with the Lu concentration data obtained by LA-ICP-MS (Fig. 5b), however, also suggest the diffusion of Lu and resorption of large parts of the garnets. Considering the small garnet diameters of Rh-89 (less than 600 μm) compared to Rh-83 (2–3 mm), garnets in Rh-89 might have been more susceptible to complete resorption and equilibration than the larger garnets in Rh-83. Furthermore, as all three eclogites from the Middle Allochthon (Rh-83, Rh-89 and Rh-197) display virtually identical Lu–Hf ages, it seems likely that the same near-peak metamorphism affecting sample Rh-83 also affected sample Rh-89.

Collectively, the Lu–Hf age of Rh-197 can be interpreted as closest representing the age of the peak metamorphic event affecting the Middle Allochthon. Samples Rh-83 and Rh-89 were affected by different degrees of garnet resorption close to the timing of the metamorphic peak. The Lu–Hf age in sample Rh-210 furthermore can be readily regarded as representative of the age of HP metamorphism in the Kardžali Unit. As mentioned above, the Sm–Nd isotope system of sample Rh-210 has been affected by element mobility during the metamorphic cycle. Therefore, we interpret the Sm–Nd age of 109 ± 11 Ma as only representing a minimum age for garnet growth.

Constraints on exhumation rates

Considering the Lu–Hf results discussed above, we can now place a robust age constraint on the P–T path of the investigated samples, in particular on the prograde flank towards peak pressure conditions (Fig. 3). Combining these results with published stratigraphic and geochronological data from the retrograde path allows to roughly estimate the orders of magnitudes of the cooling and exhumation rates. For the timing of prograde metamorphism, we use the Lu–Hf age of sample Rh-197 (42.8 ± 0.5 Ma), as it represents the youngest garnet growth age and we therefore place minimum constraints on the exhumation rate. The depth of formation inferred from phase relationships corresponds to ca. 70 km. From Ar–Ar geochronology carried out on rocks from nearby units of the Middle Allochthon, the timing of cooling below 380–320°C is constrained by ages of 37.1 ± 2.4, and 36.1 ± 0.4 Ma (Lips et al. 2000), which might be considered as minimum ages due to a relatively low blocking temperature applied by the authors (350 ± 30°C). Following Liati and Gebauer (1999), we assume a mean depth of c. 10 km for this phase of retrograde cooling. Complete exhumation of the Middle Allochthon to the surface is robustly constrained by unmetamorphosed marine sediments of Priabonian age that are unconformably resting on top of the Starcevo Unit north-east of Ardino (Yordanov et al. 2007). Hence, vertical exhumation from 70 km depth had to be accomplished within less than 8 Myr and exhumation rates are therefore around 1 cm/year, similar to values estimated for the exhumation of the Arda 1 and Starcevo Unit by Pleuger et al. (2011). This is clearly a minimum rate because the maximum subduction depths were probably reached somewhat later than the determined Lu–Hf age (<42.8 ± 0.5 Ma). Moreover, exhumation and cooling in the study area may have occurred successively, the lithologies may have been exhumed isothermally first and then cooled (Fig. 3). Collectively, the actual exhumation may probably have occurred much faster, even before cooling started. Independent of this uncertainty, our results suggest higher exhumation rates than those proposed by Liati and Gebauer (1999), in the order of 5.7–11.8 mm/year (mean of 7.7 mm/year); nevertheless, the order of magnitude is similar between both studies.

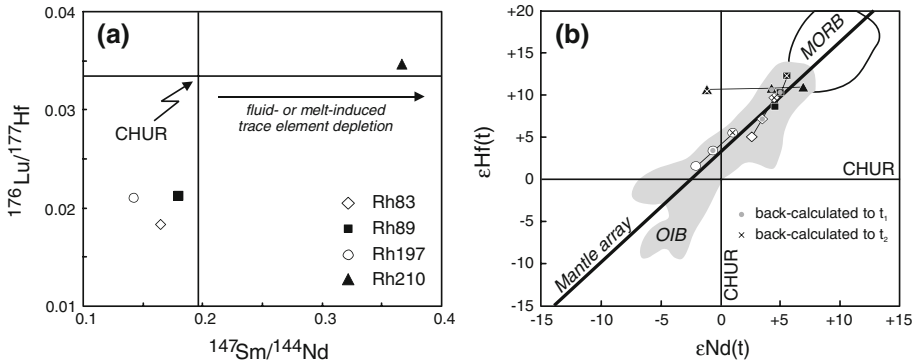

Fig. 8 Constraints on the whole rocks of the four eclogites inferred by Lu–Hf and Sm–Nd isotope systematics. **a** $^{176}Lu/^{177}Hf$ versus $^{147}Sm/^{143}Nd$ of the four eclogite samples, illustrating the effect of fluid-induced LREE depletion as it is especially important for sample Rh-210. After John et al. (2004). **b** εHf(t)–εNd(t) of the four samples in comparison with a compilation of global OIB and MORB (MORB after Pearce et al. 1999; Woodhead et al. 2001; Chauvel and Blichert-Toft 2001; Kempton et al. 2002; OIB field after Nowell et al. 1998). Each sample is shown with εHf-εNd at present day and also back-calculated to $t_1 = 250$ Ma and to $t_2 = 500$ Ma

Constraints on the magmatic protolith

In developing a palaeotectonic model for the Rhodopes, it is essential to constrain the nature of the eclogite protoliths, that is, the tectonic environment in which the eclogite precursors formed. Of importance for the present study is the distinction between a divergent (MORB), a convergent (island-/continental- or back-arc), and an intra-plate setting (e.g., OIB). In this regard, the whole rock trace element budget as well as the Hf–Nd isotope compositions serve as a valuable tool to identify the original composition of the magmatic precursor (e.g., Becker et al. 2000; John et al. 2004; Zack and John 2007; Zhao et al. 2007).

The mobility/immobility of trace elements during blueschist to eclogite transition has been the subject of extensive research over the past years where, for example, it has been shown that many trace elements are easily mobilized from the slab to the overlying mantle wedge during dehydration reactions (e.g., John et al. 2004, 2008; Zack and John 2007; Beinlich et al. 2010). However, these processes are likely limited to zones with a high fluid flux (veins, channels and other fluid pathways). Other authors proposed a decoupling of fluid and trace element flux during subduction, that is, only very limited amounts of trace elements are released from the subducting slab during prograde metamorphism (Spandler et al. 2003; 2004; 2007). Considering these interpretations, the bulk trace element patterns of the studied eclogite samples (Fig. 6a, b) may mirror element-loss of a more LREE-enriched precursor, like arc-related basalts or even OIBs, or may be considered as representative of the original magmatic protolith composition.

Sample Rh-210 from the Upper Allochthon appears to be affected by a selective loss of LILE (Cs, Rb, Ba) and LREE (La, Ce, Pr, Nd), leaving behind positive anomalies of the HFSE and HREE (see Fig. 6a, b). Evidence for either a dehydration- or partial melt-mediated dissipation of Nd and Hf in sample Rh-210 is provided by increased $^{147}Sm/^{144}Nd$ (0.3664) and $^{176}Lu/^{177}Hf$ (0.03468) when compared to the other three samples (see Fig. 8a). This feature has also major implications for the interpretation of the Sm–Nd age determined for Rh-210 (see below). In any case, the consistently low $^{147}Sm/^{144}Nd$ and $^{176}Lu/^{177}Hf$ of the samples Rh-83, Rh-89 and Rh-197 might provide some evidence that these samples preserved their original magmatic REE and HFSE compositions.

A further tool to discriminate possible tectonic settings of metamorphic protoliths are the HFSE, which are considered as relatively immobile during subduction-zone metamorphism and subsequent retrograde overprint (e.g., Kogiso et al. 1997; Becker et al. 2000; Spandler et al. 2004; Schmidt et al. 2009). Ratios like Nb/Ta and Zr/Hf (13.4–15.3 and 37.9–44.5, respectively) of the four eclogites broadly overlap the fields of N-MORB, OIB and subduction-related basaltic rocks. The derivation of the protoliths from an enriched OIB-type source however can be excluded based on the high Zr/Nb (19.4–45.1) and low Nb concentrations (<6 ppm), which would be expected to be higher if an OIB-type protolith is considered (Pfänder et al. 2007, Spandler et al. 2004). Furthermore, the negative Nb–Ta anomaly in sample Rh-197 (and to a lesser degree also in Rh-83 and Rh-89) are tentatively regarded as reflecting the derivation from a source with an island-arc setting.

Whole rock Hf (and to a lesser degree also the Nd) isotope compositions can be highly useful to constrain the nature of the eclogite protoliths due to the particular robustness of the Lu–Hf isotope system with respect to metamorphic overprints (e.g., Blichert-Toft et al. 1999; Polat et al. 2003). However, for the studied eclogites this approach is hampered by uncertainties in the protolith formation age, which is required to calculate initial isotope

compositions. Therefore, we assume a similar protolith formation age as was determined for eclogites near Sidironero by Liati (2005), reporting U–Pb SHRIMP ages for zircons of ~250 Ma (=t_1). Furthermore, a second protolith formation age (t_2) of 500 Ma was employed as a maximum estimate, as the presence of (possibly inherited) ~430-Ma-old zircon domains (Liati 2005) might indicate even older formation ages. Independent of the protolith age assumed, calculated εHf(t) and εNd(t) values for Rh-83 and Rh-197 are consistently low (see Fig. 8b), and they rather agree with the characteristics of a more enriched magmatic protolith than MORB. Conversely, initial values for Rh-89 well overlap the field for MORB. Due to the near-chondritic $^{176}Lu/^{177}Hf$ of 0.03468, the whole rock εHf value of sample Rh-210 (εHf (i) ~ +10) is rather independent of the protolith age and overlaps the lower limit of the MORB field (Fig. 8b). However, back-calculated Hf and Nd isotopes of samples Rh-83 and Rh-197 unambiguously indicate a more enriched protolith than MORB (Fig. 8b).

Collectively, our trace element and Hf–Nd isotope data for the four eclogites indicate significant element loss for sample Rh-210 and possibly preserved original magmatic trace element signatures for samples Rh-83, Rh-89 and Rh-197. We can furthermore confidently exclude an OIB-type source for all four eclogites. The protoliths of samples Rh-83, Rh-89 and Rh-197 most likely originate from an island-arc setting based on the negative Nb–Ta anomalies and the rather unradiogenic Hf–Nd isotope systematics that are inconsistent with a MORB-setting. For sample Rh-210, we propose that the modified trace element pattern (loss of LREE, Th and also low K content) as well as the elevated $^{147}Sm/^{144}Nd$ and $^{176}Lu/^{177}Hf$ is the result of a partial melting event affecting the protolith somewhat before the closure of the Lu–Hf and Sm–Nd chronometers.

Implications for the tectonics of the Rhodopes and Hellenides

Our results show that two subduction events of different age are recorded in different structural levels of the Rhodopean nappe stack: Early Cretaceous in the Upper Allochthon and Eocene in the basal part of the Middle Allochthon. Such a distribution, older ages in the structurally higher nappes and younger ages in the deeper levels, is typical for collisional orogens and is also seen, for example, in the Alps (e.g., Gebauer 1999) and the Norwegian Caledonides (e.g., Brueckner and Van Roermund 2004). Our geochronological study confirms the results of Liati and Gebauer (1999) and Liati (2005) from U–Pb zircon dating, in that subduction-related metamorphism in the Rhodopes occurred more than once. In earlier studies, however, the geochronological results were rather assigned to specific areas (e.g., Western Rhodopes, Central Rhodopes—Liati 2005) and not to specific structural levels in the Rhodopean nappe stack. In the present study, we connect the results of the geochronology with the respective tectonostratigraphy, an approach that has emerged in the last few years (Krohe and Mposkos 2002). It is also important to emphasize that our data actually support two metamorphic events (Early Cretaceous and Eocene), but do not preclude the existence of other subduction events, for example, in the Jurassic (Liati 2005; Bauer et al. 2007; Krenn et al. 2010; Nagel et al. 2011), at a more regional scale.

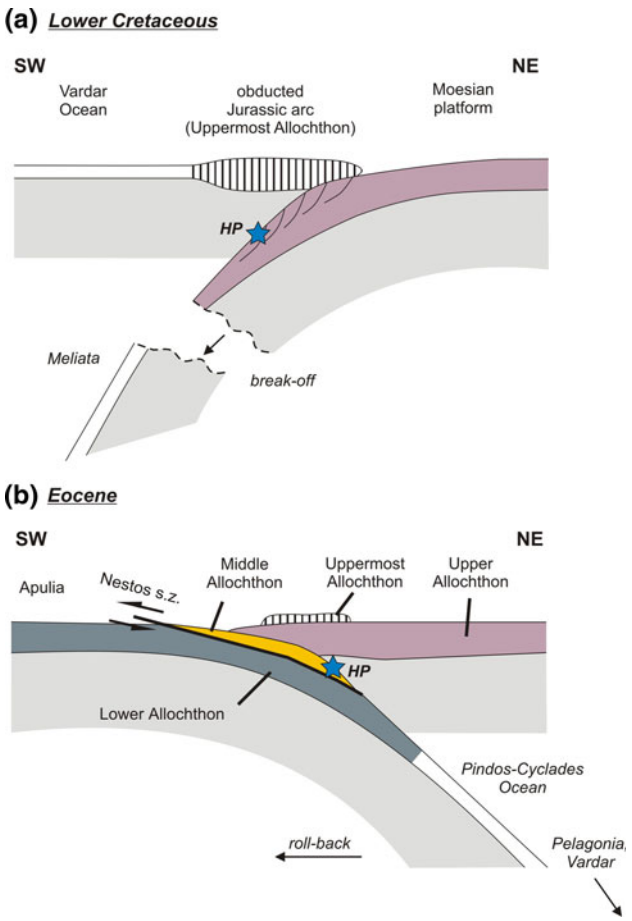

Fig. 9 Schematic sketch illustrating the proposed palaeotectonic reconstruction of the Rhodope nappe stack for **a** the Lower Cretaceous and **b** the Eocene. Modified after Jahn-Awe et al. (2011)

Significance of the Eocene ages from the Middle Allochthon

According to the most widely accepted evolutionary models for the Hellenic-Aegean orogenic system (van Hinsbergen et al. 2005; Papanikolaou 2009; Jolivet and Brun 2010), subduction and related metamorphism and deformation migrated progressively southwards during the Mesozoic and Cenozoic. These models have assumed that

the stacking of the Rhodopean nappes is Cretaceous in age. It has also been assumed that from the end of the Cretaceous onward, the Rhodopes were already in the hinterland of the southward-retreating subduction zone (e.g., von Quadt et al. 2005) and thus were only affected by HT metamorphism, magmatism and exhumation. However, this view cannot be maintained any longer. Instead, the basal part of the Middle Allochthon records subduction in the Eocene. Eocene ages for the peak pressure were already determined by U–Pb zircon SHRIMP dating of kyanite-eclogites from the area of Thermes in northern Greece (42.2 ± 9 Ma; Liati and Gebauer 1999). The results presented in our study thus confirm the inferences of Liati and Gebauer (1999). In the Nestos Shear Zone near Sidironero, further west but still in the same structural level, Liati (2005) dated the HP stage of an amphibolitized eclogite to 51.0 ± 1.0 Ma. Our new Eocene ages (44.6 ± 0.7 Ma, 43.5 ± 0.4 Ma, 42.8 ± 0.5 Ma) partially fill the gap between the ages from Thermes and from Sidironero. Hence, we assume that the ages from Thermes and Sidironero do not represent different metamorphic events, as suggested by Liati (2005), but rather point to protracted subduction lasting at least between 51 and 42 Ma. During the course of this subduction episode, different parts of the Middle Allochthon appear to have reached their peak pressure at different times.

Given the age constraints above, the question arises in which subduction zone system, from a palaeogeographic point of view, the Eocene eclogites of the Rhodopes formed. All of the Eocene eclogites are from the lower part of the Middle Allochthon. This tectonic unit disappears beneath the Upper Allochthon towards the south-west. It is unlikely that the Middle Allochthon re-emerges in the ophiolite-bearing Vardar Zone, adjacent to the Rhodopes to the SW, as no Eocene HP metamorphism is known from that area. In the Cycladic Blueschist Unit, however, which is derived from the more south-westerly located Pindos-Cyclades Ocean, eclogite-facies metamorphism is also Eocene in age (U–Pb zircon and Lu–Hf garnet ages from 50 to 52 Ma; Tomaschek et al. 2003; Lagos et al. 2007). From stratigraphic evidence, ophiolites from the Pindos-Cyclades ocean were emplaced towards south-west onto continental crust of the Apulian continent during the Middle to Late Eocene (Papanikolaou 2009). The emplacement of the Middle on the Lower Allochthon of the Rhodopes is also of Middle to Late Eocene age, as it postdates ca. 43 Ma old eclogite-facies metamorphism in the Middle Allochthon (this study, Nagel et al. 2011), and predates granitoid intrusions at 32 Ma (Jahn-Awe et al. 2010). Therefore, we suggest that the base of the Middle Allochthon in the Rhodopes represents the continuation of the Pindos-Cyclades suture towards deeper levels. In consequence, the underlying Lower Allochthon is correlated with the continental crust of Apulia (External Hellenide carbonate platform), as suggested by Dinter (1998), Krohe and Mposkos (2002), Jahn-Awe et al. (2010), and as illustrated in a palaeotectonic sketch map in Fig. 9b. The Rhodopes are therefore interpreted as a large-scale tectonic window, exposing in its core the deepest nappe units of the Hellenides (see also Mposkos and Krohe 2000). The sutures of both the Vardar and Pindos-Cyclades oceans are rooted along the northern border of the Rhodopes, north of the metamorphic domes (Arda).

Significance of the Early Cretaceous age from the Upper Allochthon

The new 126.0 ± 0.7 Ma age for the eclogite from the Upper Allochthon is similar to published ages from the Kimi Complex (119.0 ± 3.5 Ma, Sm–Nd age for a garnet-pyroxenite; Wawrzenitz and Mposkos 1997; and 117.4 ± 1.9, U–Pb zircon SHRIMP age for a garnet-rich mafic rock; Liati et al. 2002) and indicates that the Upper Allochthon in the Eastern Rhodopes was subducted during the Early Cretaceous. We assume that the Upper Allochthon represents the continental margin of Europe (Moesia), which collided with a Jurassic arc formed above a south-west-dipping subduction zone that consumed the Meliata Ocean (Bonev and Stampfli 2008; Jahn-Awe et al. 2010; see Fig. 9a). During and after this collision, the European margin entered the subduction zone and was affected by eclogite-facies metamorphism. Between the Lower Cretaceous and the Eocene HP metamorphism, a subduction polarity switch occurred and the kinematic framework changed fundamentally.

Conclusions

New combined petrological and geochronological data for metamorphic rocks from the Bulgarian section of the Rhodopes can place new constrains on the tectonic evolution of the Eastern Mediterranean region. Lu–Hf garnet geochronological results for four eclogites from the Middle and Upper Allochthon reveal two high-pressure metamorphic events: (1) in the Lower Cretaceous (126 Ma) for the Upper Allochthon and (2) in the Eocene (45–42 Ma) for the Middle Allochthon. Geothermobarometry can place the peak metamorphic conditions in the Middle Allochthon at c. 700°C/20–25 kbar. Major and trace element analyses of the whole rocks point to an island-arc origin of the samples from the Middle Allochthon and clearly exclude OIB-like protoliths. Our data furthermore support previous findings that the Rhodopes represent a large-scale tectonic window, emphasizing a key role of the Rhodopes to understand the tectonic evolution of the Hellenides.

Acknowledgments The authors are very grateful to Dieter Garbe-Schönberg, Ulrike Westernströer and the technical staff of the ICPMS lab at CAU Kiel for trace element measurements. Furthermore, Radegund Hoffbauer, Universität Bonn, is thanked for XRF analyses. We also thank D. Herwartz and J. E. Hoffmann for constructive discussions and help in the laboratory and V. Laurenz for assistance during electron microprobe measurements. We also thank J.-P. Burg, E. Moulas and N. Georgiev for discussions. This work greatly benefited from the reviews of Jan Kramers, Susanne Skora and an anonymous reviewer. Editorial handling by Jochen Hoefs was highly appreciated. Funding by DFG (Deutsche Forschungsgemeinschaft) grants BR1909/8-1 and Mu1490/9-2 to CM and FR700/10 to NF are highly acknowledged.

References

Amato JM, Johnson CM, Baumgartner LP, Beard BL (1999) Rapid exhumation of the Zermatt-Saas ophiolite deduced from high-precision Sm-Nd and Rb-Sr geochronology. Earth Planet Sci Lett 171:425–438

Bauer C, Rubatto D, Krenn K, Proyer A, Hoinkes G (2007) A zircon study from the Rhodope metamorphic complex, N-Greece: time record of a multistage evolution. Lithos 99:207–228

Baziotis I, Mposkos E, Asimow PD (2008) Petrogenesis of ultramafic rocks from the ultrahigh-pressure metamorphic Kimi Complex in Eastern Rhodope (NE Greece). J Petrol 49:885–909

Becker H, Jochum KP, Carlson RW (2000) Trace element fractionation during dehydration of eclogites from high-pressure terranes and the implications for element fluxes in subduction zones. Chem Geol 163:65–99

Beinlich A, Klemd R, John T, Gao J (2010) Trace-element mobilization during Ca-metasomatism along a major fluid conduit: Eclogitization of blueschist as a consequence of fluid-rock interaction. Geochim Cosmochim Acta 74:1892–1922

Berman RG (1988) Internally-consistent thermodynamic data for minerals in the system Na2O-K2O-CaO-MgO-Fe2O3-Al2O3-SiO2-TiO2-H2O-CO2. J Petrol 29:445–522

Berman RG (1990) Mixing properties of Ca-Mg-Fe-Mn garnets. Am Mineral 75:328–344

Bizzarro M, Baker JA, Haack H, Ulfbeck D, Rosing M (2003) Early history of Earth's crust-mantle system inferred from hafnium isotopes in chondrites. Nature 421:931–933

Blichert-Toft J, Frei R (2001) Complex Sm-Nd and Lu-Hf isotope systematics in metamorphic garnets from the Isua supracrustal belt, West Greenland. Geochim Cosmochim Acta 65:3177–3187

Blichert-Toft J, Albarède F, Rosing M, Frei R, Bridgwater D (1999) The Nd and Hf isotopic evolution of the mantle through the Archean. Results from the Isua supracrustals, West Greenland, and from the Birimian terranes of West Africa. Geochim Cosmochim Acta 63:3901–3914

Bonev N, Stampfli G (2003) New structural and petrologic data on Mesozoic schists in the Rhodope (Bulgaria): geodynamic implications. C R Geosci 335:691–699

Bonev N, Stampfli G (2008) Petrology, geochemistry and geodynamic implications of Jurassic island arc magmatism as revealed by mafic volcanic rocks in the Mesozoic low-grade sequence, eastern Rhodope, Bulgaria. Lithos 100:210–233

Bonev N, Burg J-P, Ivanov Z (2006) Mesozoic-Tertiary structural evolution of an extensional gneiss dome—the Kesebir-Kardamos dome, eastern Rhodope (Bulgaria-Greece). Int J Earth Sci 95:318–340

Bosse V, Boulvais P, Gautier P, Tiepolo M, Ruffet G, Devidal JL, Cherneva Z, Gerdjikov I, Paquette JL (2009) Fluid-induced disturbance of the monazite Th-Pb chronometer: in situ dating and element mapping in pegmatites from the Rhodope (Greece, Bulgaria). Chem Geol 261:286–302

Brueckner HK, van Roermund HLM (2004) Dunk tectonics: a multiple subduction/eduction model for the evolution of the Scandinavian Caledonides. Tectonics 23:TC2004

Büchl A, Münker C, Mezger K, Hofmann AW (2002) High-precision Nb/Ta and Zr/Hf ratios in global MORB. Geochim Cosmochim Acta 66(15A):A108

Burg J-P, Ivanov Z, Ricou L-E, Dimor D, Klain L (1990) Implications of shear-sense criteria for the tectonic evolution of the Central Rhodope massif, southern Bulgaria. Geology 18:451–454

Burg J-P, Ricou LE, Ivanov Z, Godfriaux I, Dimov D, Klain L (1996) Syn-metamorphic nappe complex in the Rhodope massif: structure and kinematics. Terra Nova 8:6–15

Caddick MJ, Konopásek J, Thompson AB (2010) Preservation of garnet growth zoning and the duration of prograde metamorphism. J Petrol 51:2327–2347

Carrigan CW, Essene EJ, Mukasa SB, Kolcheva K, Haydoutov I, Carpenter CM (2002) Thermobarometric constraints on the formation of sapphirine-spinel-plagioclase symplectites in kyanite eclogites, and the prograde and retrograde P–T path, central Rhodope massif, Bulgaria. Geological Society of America Denver Annual Meeting, paper no 220–10

Chakraborty S, Rubie DC (1996) Mg tracer diffusion in aluminosilicate garnets at 750–850°C, 1 atm and 1, 300°C, 8.5 GPa. Contrib Mineral Petrol 122:406–414

Chauvel C, Blichert-Toft J (2001) A hafnium isotope and trace element perspective on melting of the depleted mantle. Earth Planet Sci Lett 190:137–151

Cherneva Z, Ovtcharova M, von Quadt A, Kolcheva K, Stancheva E, Sarov S, Peytcheva I (2002) Monazite and zircon U–Pb ages of migmatites from Arda River Valley, Central Rhodopian Dome, Bulgaria. In: Proceedings of the annual scientific conference of BGS, Sofia, pp 20–22

Cornelius NK (2008) UHP metamorphic rocks of the Eastern Rhodope Massif, NE Greece: new constraints from petrology, geochemistry and zircon ages. Dissertation, Johannes Gutenberg-Universität Mainz

De Capitani C, Petrakakis K (2010) The computation of equilibrium assemblage diagrams with Theriak/Domino software. Am Mineral 95:1006–1016

Dinter DA (1998) Late Cenozoic extension of the Alpine collisional orogen, northeastern Greece: origin of the north Aegean basin. GSA Bull 110:1208–1230

Dinter DA, Royden L (1993) Late Cenozoic extension in northeastern Greece: Strymon Valley detachment and Rhodope metamorphic core complex. Geology 21:45–48

Duchêne S, Blichert-Toft J, Luais B, Telouk P, Lardeaux JM, Albarède F (1997) The Lu-Hf dating of garnets and the ages of the Alpine high-pressure metamorphism. Nature 387:586–589

Dutch R, Hand M (2010) Retention of Sm-Nd isotopic ages in garnets subjected to high-grade thermal reworking: implications for diffusion rates of major and rare earth elements and the Sm-Nd closure temperature in garnet. Contrib Mineral Petrol 159:93–112

Fuhrman ML, Lindsley DH (1988) Ternary feldspar modelling and thermometry. Am Mineral 73:201–215

Ganguly J, Tirone M, Hervig RL (1998) Diffusion kinetics of samarium and neodymium in garnet, and a method for determining cooling rates of rocks. Science 281:805–807

Garbe-Schönberg C-D (1993) Simultaneous determination of thirty-seven trace elements in twenty-eight international rock standards by ICP-MS. Geostand Geoanal Res 17:81–97

Gebauer D (1999) Alpine geochronology of the Central and Western Alps: new constraints for a complex geodynamic evolution. Schweiz Miner Petrog Mitt 79:191–208

Gebauer D, Schertl H-P, Brix M, Schreyer W (1997) 35 Ma old ultrahigh-pressure metamorphism and evidence for very rapid exhumation in the Dora Maira Massif, Western Alps. Lithos 41:5–24

Georgiev N, Pleuger J, Froitzheim N, Sarov S, Jahn-Awe S, Nagel TJ (2010) Separate Eocene-Early Oligocene and Miocene stages of extension and core complex formation in the Western Rhodopes, Mesta Basin, and Pirin Mountains (Bulgaria). Tectonophysics 487:59–84

Georgieva M, Cherneva Z, Kolcheva K, Sarov S, Gerdjikov I, Voinova E (2002) P–T metamorphic path of silimanite-bearing schists in an extensional shear zone, Central Rhodopes, Bulgaria. Geochem Mineral Petrol 39:95–106

Gerdjikov I, Gautier P, Cherneva Z, Bosse V, Ruffet G (2010) Late Eocene synmetamorphic thrusting and synorogenic extension across the metamorphic pile of the Bulgarian Central Rhodope. Geol Balc 39:132–133

Herwartz D, Münker C, Scherer EE, Nagel TJ, Pleuger J, Froitzheim N (2008) Lu-Hf garnet geochronology of eclogites from the Balma Unit (Pennine Alps): implications for Alpine paleotectonic reconstructions. Swiss J Geosci 101:S173–S189

Herwartz D, Nagel TJ, Münker C, Scherer EE, Froitzheim N (2011) Tracing two orogenic cycles in one eclogite sample by Lu-Hf garnet chronometry. Nat Geosci. doi:10.1038/ngeo1060

Himmerkus F, Reischmann T, Kostopoulos D (2009a) Triassic rift-related meta-granites in the Internal Hellenides, Greece. Geol Mag 146:252–265

Himmerkus F, Reischmann T, Kostopoulos D (2009b) Serbo-Macedonian revisited: a Silurian basement terrane from northern Gondwana in the Internal Hellenides, Greece. Tectonophysics 473:20–35

Holland TJB, Powell R (1998) An internally consistent thermodynamic data set for phases of petrological interest. J Metamorph Geol 16:309–343

Jahn-Awe S, Froitzheim N, Nagel TJ, Frei D, Georgiev N, Pleuger J (2010) Structural and geochronological evidence for Paleogene thrusting in the western Rhodopes, SW Bulgaria: elements for a new tectonic model of the Rhodope Metamorphic Province. Tectonics 29:TC3008

Jahn-Awe S, Pleuger J, Frei D, Georgiev N, Froitzheim N, Nagel TJ. (2011) Time constraints for low-angle shear zones in the Central Rhodopes (Bulgaria) and their significance for the exhumation of high-pressure rocks. Int J Earth Sci (accepted)

Janák M, Froitzheim N, Georgiev N, Nagel TJ, Sarov S (2011) P-T evolution of kyanite eclogite from the Pirin Mountains (SW Bulgaria): implications for the Rhodope UHP Metamorphic Complex. J Metamorph Geol 29:317–332

John T, Scherer EE, Haase K, Schenk V (2004) Trace element fractionation during fluid-induced eclogitization in a subducting slab: trace element and Lu-Hf-Sm-Nd isotope systematics. Earth Planet Sci Lett 227:441–456

John T, Klemd R, Gao J, Garbe-Schönberg CD (2008) Trace-element mobilization in slabs due to non steady-state fluid-rock interaction: Constraints from an eclogite-facies transport vein in blueschist (Tianshan, China). Lithos 103:1–24

Jolivet L, Brun J-P (2010) Cenozoic geodynamic evolution of the Aegean. Int J Earth Sci 99:109–138

Kelly ED, Carlson WD, Connelly JN (2011) Implications of garnet resorption for the Lu-Hf garnet geochronometer: an example from the contact aureole of the Makhavinekh Lake Pluton, Labrador. J Metamorph Geol 8:901–916

Kempton PD, Pearce JA, Barry TL, Fitton JG, Langmuir C, Christie DM (2002) Sr-Nd-Pb-Hf isotope results from ODP Leg 187: evidence for mantle dynamics of the Australian-Antarctic discordance and origin of the Indian MORB source. Geochem Geophys Geosys 3. doi:10.1029/2002GC000320

Kilias A, Falalakis G, Mountrakis D (1999) Cretaceous-Tertiary structures and kinematics of the Serbomacedonian metamorphic rocks and their relation to the exhumation of the Hellenic Hinterland (Macedonia, Greece). Int J Earth Sci 88:513–531

Kogiso T, Tatsumi Y, Nakano S (1997) Trace element transport during dehydration processes in the subducted oceanic crust. 1. Experiments and implications for the origin of ocean island basalts. Earth Planet Sci Lett 148:193–205

Kohn MJ (2003) Geochemical zoning in metamorphic minerals. In: Rudnick RL (ed) The crust, treatise of geochemistry, vol 3. Elsevier, Pergamon, pp 229–262

Kohn MJ (2009) Models of garnet differential geochronology. Geochim Cosmochim Acta 73:170–182

Kolčeva K, Željažkova-Panajotova M, Dobrecov NL, Stojanova V (1986) Eclogites in the Rhodope Metamorphic group and their retrograde metamorphism. Geochem Mineral Petrol 20–21:130–144

Krenn K, Bauer C, Proyer C, Klötzli U, Hoinkes G (2010) Tectonometamorphic evolution of the Rhodope orogen. Tectonics 29:TC4001

Krohe A, Mposkos E (2002) Multiple generations of extensional detachments in the Rhodope Mountain (Northern Greece): evidence of episodic exhumation of high-pressure rocks. In: Blundell D, Neubauer F, von Quadt A (eds) The timing and location of major ore deposits in an evolving orogen. Geol Soc London Spec Pub 206:151–178

Lagos M, Scherer EE, Tomaschek F, Münker C, Keiter M, Berndt J, Ballhaus C (2007) High precision Lu-Hf geochronology of Eocene eclogite-facies rocks from Syros, Cyclades, Greece. Chem Geol 243:16–35

Lapen TJ, Johnson CM, Baumgartner LP, Mahlen NJ, Beard BL, Amato JM (2003) Burial rates during prograde metamorphism of an ultra-high-pressure terrane: an example from Lago di Cignana, western Alps, Italy. Earth Planet Sci Lett 215:57–72

Liati A (2005) Identification of repeated Alpine (ultra) high-pressure metamorphic events by U-Pb SHRIMP geochronology and REE geochemistry of zircon: the Rhodope zone of Northern Greece. Contrib Mineral Petrol 150:608–630

Liati A, Gebauer D (1999) Constraining the prograde and retrograde P-T-t path of Eocene HP rocks by SHRIMP dating of different zircon domains: inferred rates of heating, burial, cooling and exhumation for central Rhodope, northern Greece. Contrib Mineral Petrol 135:340–354

Liati A, Mposkos E (1990) Evolution of the eclogites in the Rhodope Zone of northern Greece. Lithos 25:89–99

Liati A, Seidel E (1996) Metamorphic evolution and geochemistry of kyanite eclogites in central Rhodope, northern Greece. Contrib Mineral Petrol 123:293–307

Liati A, Gebauer D, Wysoczanski R (2002) U-Pb SHRIMP-dating of zircon domains from UHP garnet-rich mafic rocks and late pegmatoids in the Rhodope zone (N Greece); evidence for Early Cretaceous crystallization and Late Cretaceous metamorphism. Chem Geol 184:281–299

Lips ALW, White SH, Wijbrans JR (2000) Middle-Late Alpine thermotectonic evolution of the southern Rhodope massif, Greece. Geodin Acta 13:281–292

Longerich HP, Jackson SE, Günther D (1996) Laser ablation inductively coupled plasma mass spectrometric transient signal data acquisition and analyte concentration calculation. J Anal Atom Spectrom 11:899–904

Ludwig KR (2001) Isoplot/Ex version 2.49, Geochronological toolkit for microsoft excel. Berkeley Geochron Center Spec Pub 1a

Massonne HJ, Szpurka Z (1997) Thermodynamic properties of white mica on the basis of high-pressure experiments in the system K2O-MgO-Al2O3-SiO2-H2O and K2O-FeO-Al2O3-SiO2-H2O. Lithos 41:229–250

Mposkos E, Wawrzenitz N (1995) Metapegmatites and pegmatites bracketing the time of HP-metamorphism in polymetamorphic rocks of the E. Rhodope, N. Greece: petrological and geochronological constraints. Geological Society of Greece, Special Publication, vol 4, pp 602–608

Mposkos ED, Kostopoulos DK (2001) Diamond, former coesite and supersilicic garnet in metasedimentary rocks from the Greek Rhodope: a new ultrahigh-pressure metamorphic province established. Earth Planet Sci Lett 192:497–506

Mposkos ED, Krohe A (2000) Petrological and structural evolution of continental high pressure (HP) metamorphic rocks in the Alpine Rhodope Domain (N. Greece). In: Panayides I, Xenophontos C, Malpas J (eds) Proceedings of the 3rd international conference on the geology of the eastern mediterranean, Nicosia, Cyprus, pp 221–232

Münker C, Weyer S, Scherer EE, Mezger K (2001) Separation of high field strength elements (Nb, Ta, Zr, Hf) and Lu from rock samples for MC-ICPMS measurements. Geochem Geophys Geosys 2. doi:10.1029/2001GC000183

Münker C, Wörner G, Yogodzinski G, Churikova T (2004) Behaviour of high field strength elements in subduction zones: constraints from Kamchatka-Aleutian arc lavas. Earth Planet Sci Lett 224:275–293

Nagel TJ, Schmidt S, Janák M, Froitzheim N, Jahn-Awe S, Georgiev N (2011) The exposed base of a collapsing wedge—the Nestos Shear Zone (Rhodope Metamorphic Province, Greece). Tectonics. doi:10.1029/2010TC002815

Nowell GM, Kempton PD, Noble SR, Fitton JG, Saunder AD, Mahoney JJ, Taylor RN (1998) High precision Hf isotope measurements of MORB and OIB by thermal ionisation mass spectrometry: insights into the depleted mantle. Chem Geol 149:211–233

Ovtcharova M, von Quadt AV, Cherneva Z, Sarov S, Heinrich C, Peytcheva I (2004) U-Pb dating of zircon and monazite from granitoids and migmatites in the core and eastern periphery of the Central Rhodopean Dome, Bulgaria. Geochim Cosmochim Acta 68:A664

Papanikolaou D (2009) Timing of tectonic emplacement of the ophiolites and terrane paleogeography in the Hellenides. Lithos 108:262–280

Pearce NJG, Perkins WT, Westgate JA, Gorton MP, Jackson SE, Neal CR, Chenery SP (1997) A compilation of new and published major and trace element data for NIST SRM 610 and NIST SRM 612 glass reference materials. Geost Newslett 21:115–144

Pearce JA, Kempton PD, Nowell GM, Noble SR (1999) Hf-Nd element and isotope perspective on the nature and provenance of mantle and subduction components in Western Pacific arc-basin systems. J Petrol 40:1579–1611

Perraki M, Proyer A, Mposkos E, Kaindl R, Hoinkes G (2006) Raman micro-spectroscopy on diamond, graphite and other carbon polymorphs from the ultrahigh-pressure metamorphic Kimi Complex of the Rhodope Metamorphic Province, NE Greece. Earth Planet Sci Lett 241:672–685

Peytcheva I, von Quadt A, Ovtcharova M, Handler R, Neubauer F, Salnikova E, Kostitsyn Y, Sarov S, Kolcheva K (2004) Metagranitoids from the eastern part of the Central Rhodopean Dome (Bulgaria): U-Pb, Rb-Sr and $^{40}Ar/^{39}Ar$ timing of emplacement and exhumation and isotope-geochemical features. Mineral Petrol 82:1–31

Pfänder JA, Münker C, Stracke A, Mezger K (2007) Nb/Ta and Zr/Hf in ocean island basalts—Implications for crust-mantle differentiation and the fate of Niobium. Earth Planet Sci Lett 254:158–172

Pin C, Zalduegui JFS (1997) Sequential separation of light rare-earth elements, thorium and uranium by miniaturized extraction chromatography: application to isotopic analyses of silicate rocks. Anal Chim Acta 339:79–89

Pleuger J, Georgiev N, Jahn-Awe S, Froitzheim N, Valkanov N (2011) Kinematics of Palaeogene low-angle extensional faults and basin formation along the eastern border of the Central Rhodopes (Bulgaria). Z dt Ges Geowiss 162:171–192

Polat A, Hofmann AW, Münker C, Regelous M, Appel PWU (2003) Contrasting geochemical patterns in the 3.7–3.8 Ga pillow basalt cores and rims, Isua greenstone belt, Southwest Greenland: Implications for postmagmatic alteration processes. Geochim Cosmochim Acta 67:441–457

Ricou L-E, Burg J-P, Godfriaux I, Ivanov Z (1998) Rhodope and Vardar: The metamorphic and the olistostromic paired belts related to the Cretaceous subduction under Europe. Geodin Acta 11:285–309

Scherer EE, Cameron KL, Johnson CM, Beard BL, Barovich KM, Collerson KD (1997) Lu-Hf geochronology applied to dating Cenozoic events affecting lower crustal xenoliths from Kilbourne Hole, New Mexico. Chem Geol 142:63–78

Scherer EE, Cameron KL, Blichert-Toft J (2000) Lu-Hf garnet geochronology: closure temperature relative to the Sm-Nd system and the effects of trace mineral inclusions. Geochim Cosmochim Acta 64:3413–3432

Scherer EE, Münker C, Mezger K (2001) Calibration of the Lutetium-Hafnium clock. Science 293:683–687

Schmidt A, Weyer S, John T, Brey GP (2009) HFSE systematics of rutile-bearing eclogites: New insights into subduction zone processes and implications for the earth's HFSE budget. Geochim Cosmochim Acta 73:455–468

Schmidt S, Nagel TJ, Froitzheim N (2010) A new occurrence of microdiamond-bearing metamorphic rocks, SW Rhodopes, Greece. Eur J Mineral 22:189–198

Skora S, Baumgartner LP, Mahlen NJ, Johnson CM, Pilet S, Hellebrand E (2006) Diffusion-limited REE uptake by eclogite garnets and its consequences for Lu-Hf and Sm-Nd geochronology. Contrib Mineral Petrol 152:703–720

Skora S, Lapen TJ, Baumgartner LP, Johnson CM, Hellebrand E, Mahlen NJ (2009) The duration of prograde garnet crystallization in the UHP eclogites at Lago di Cignana, Italy. Earth Planet Sci Lett 287:402–411

Smit MA, Scherer EE, Bröcker M, van Roermund HLM (2010) Timing of eclogite facies metamorphism in the southernmost Scandinavian Caledonides by Lu-Hf and Sm-Nd geochronology. Contrib Mineral Petrol 159:521–539

Söderlund U, Patchett PJ, Vervoort JD, Isachsen CE (2004) The 176Lu decay constant determined by Lu-Hf and U-Pb isotope systematics of Precambrian mafic intrusions. Earth Planet Sci Lett 219:311–324

Spandler C, Hermann J, Arculus R, Mavrogenes J (2003) Redistribution of trace elements during prograde metamorphism from lawsonite blueschist to eclogite facies; implications for deep subduction-zone processes. Contrib Mineral Petrol 146:205–222

Spandler C, Hermann J, Arculus R, Mavrogenes J (2004) Geochemical heterogeneity and element mobility in deeply subducted oceanic crust; insights from high-pressure mafic rocks from New Caledonia. Chem Geol 206:21–42

Spandler C, Mavrogenes J, Hermann J (2007) Experimental constraints on element mobility from subducted sediments using high-P synthetic fluid/melt inclusions. Chem Geol 239:228–249

Stampfli GM, Borel GD (2002) A plate tectonic model for the Paleozoic and Mesozoic constrained by dynamic plate boundaries and restored synthetic oceanic isochrons. Earth Planet Sci Lett 196:17–33

Sun S-s, McDonough WF (1989) Chemical and isotopic systematics of oceanic basalts: implications for mantle composition and

processes. In: Saunders AD, Norry MJ (eds) Magmatism in the Ocean Basins. Geol Soc Spec Pub 42:313–345

Thöni M (2002) Sm-Nd isotope systematics in garnet from different lithologies (Eastern Alps): age results, and an evaluation of potential problems for garnet Sm-Nd chronometry. Chem Geol 185:255–281

Tomaschek F, Kennedy AK, Villa IM, Lagos M, Ballhaus C (2003) Zircons from Syros, Cyclades, Greece–Recrystallization and Mobilization of Zircon during High-Pressure Metamorphism. J Petrol 44:1977–2002

Tueckmantel C, Schmidt S, Neisen M, Georgiev N, Nagel TJ, Froitzheim N (2008) The Rila-Pastra Normal Fault and multi-stage extensional unroofing in the Rila Mountains (SW Bulgaria). Swiss J Geosci 101:S295–S310

Turpaud P, Reischmann T (2010) Characterization of igneous terranes by zircon dating: implications for UHP occurrences and suture identification in the Central Rhodope, northern Greece. Int J Earth Sci 99:567–591

van Hinsbergen DJJ, Hafkenscheid E, Spakman W, Meulenkamp JE, Wortel R (2005) Nappe stacking resulting from subduction of oceanic and continental lithosphere below Greece. Geology 33:325–328

van Orman JA, Grove TL, Shimizu N, Layne GD (2002) Rare earth element diffusion in a natural pyrope single crystal at 2.8 GPa. Contrib Mineral Petrol 142:416–424

Vance D, O'Nions RK (1990) Isotopic chronometry of zoned garnets: growth kinetics and metamorphic histories. Earth Planet Sci Lett 97:227–240

von Quadt A, Moritz R, Peytcheva I, Heinrich CA (2005) Geochronology and geodynamics of Late Cretaceous magmatism and Cu-Au minerlization in the Panagyurishte region of the Apuseni-Banat-Timok-Srednogorie belt, Bulgaria. Ore Geol Rev 27:95–126

Wawrzenitz N, Mposkos E (1997) First evidence for Lower Cretaceous HP/HT-metamorphism in the Eastern Rhodope, North Aegean Region, North-East Greece. Eur J Mineral 9:659–664

Woodhead JD, Hergt JM, Davidson JP, Eggins SM (2001) Hafnium isotope evidence for 'conservative' element mobility during subduction zone processes. Earth Planet Sci Lett 192:331–346

Yordanov B, Sarov S, Georgiev S, Dobrev G, Grozdev V, Balkanska E, Moskovska L (2007) Geological map of Bulgaria 1:50000, Map sheet K-35-75-B Komuniga, with explanatory notes. Geology and Geophysics Ltd, Sofia

Zack T, John T (2007) An evaluation of reactive fluid flow and trace element mobility in subducting slabs. Chem Geol 239:199–246

Zhao Z-F, Zheng Y-F, Chen R-X, Xia Q-X, Wu W-B (2007) Element mobility in mafic and felsic ultrahigh-pressure metamorphic rocks during continental collision. Geochim Cosmochim Acta 71:5244–5266